JOURNAL OF GEOPHYSICAL RESEARCH, VOL. 98, NO. B3, PAGES 4509–4526, MARCH 10, 1993

Present-Day Secular Variations in the Zonal Harmonics of Earth's Geopotential

J. X. MITROVICA[1]

Harvard Smithsonian Center for Astrophysics, Cambridge, Massachusetts

W. R. PELTIER

Department of Physics, University of Toronto, Toronto, Ontario, Canada

We develop a new formalism for the prediction of secular variations in the gravitational potential field of a spherically symmetric, self-gravitating, (Maxwell) viscoelastic planetary model subjected to an arbitrary surface load which may include a gravitationally self-consistent ocean loading component. The theory is applied to generate the most accurate predictions to date, of the present-day secular variations in the zonal harmonics of the geopotential (the so-called $\dot{J}_\ell$ for degree ℓ) arising as a consequence of the late Pleistocene glacial cycles. In this respect, we use the very recent ICE-3G reconstruction of the last late Pleistocene deglaciation event (Tushingham and Peltier, 1991). A comparison of these predictions with those generated using simplified disk models of the ice sheets, which have been used in all previous studies of the $\dot{J}_\ell$ harmonics ($\ell > 2$), indicates that the disk model approximation introduces unacceptably large errors at all spherical harmonic degrees except perhaps ℓ=2. Predictions have also been made using a eustatic loading approximation (also used in previous studies) in place of a gravitationally self-consistent ocean loading component, and we have found that the resulting discrepancy is largest at degrees 2, 8 and 10. In the case of $\dot{J}_2$ the magnitude of the error incurred using the eustatic approximation can be as large as order 10-15% of the predicted value. We have attributed this discrepancy to the present day net flux of water away from the equatorial regions arising from the remnant present-day adjustment associated with the late Pleistocene glacial cycles. The effect represents a heretofore unrecognized contribution to the $\dot{J}_\ell$ harmonics, or alternatively the nontidal acceleration of Earth's axial rate of rotation. In terms of the latter, the maximum anomaly in the length of day is approximately 1.7 μs/yr. We also consider the sensitivity of the $\dot{J}_\ell$ data to variations in the radial mantle viscosity profile by using a suite of forward calculations and an examination of Fréchet kernels. The theory required for the computation of those kernels is described herein. We find that the radial variation in sensitivity can be a strong function of the viscosity model used in the calculations. For models with a uniform upper mantle viscosity (ν_{UM}) of 10^{21} Pa s, forward predictions of the $\dot{J}_\ell$ harmonics exhibit a pronounced peak when a wide enough range of lower mantle viscosities (ν_{LM}) are considered (we denote the ν_{LM} value at this peak as $\hat{\nu}^\ell_{LM}$). At the lowest degrees ($\ell \leq 4$), Fréchet kernels computed for a series of increasing ν_{LM} values (10^{21} Pa s $\leq \nu_{LM} < 10^{23}$ Pa s) indicate a migration of the dominant sensitivity of the $\dot{J}_\ell$ data to variations in viscosity from regions below approximately 1200 km depth (for $\nu_{LM} \leq \hat{\nu}^\ell_{LM}$) to regions above this depth in the lower mantle (for $\nu_{LM} \geq \hat{\nu}^\ell_{LM}$). The sensitivity of the $\dot{J}_\ell$ data to variations in the viscosity profile in the shallowest parts of the lower mantle, for the case $\nu_{LM} \geq \hat{\nu}^\ell_{LM}$, is also reflected in a set of forward calculations described herein. As an example, $\dot{J}_\ell$ predictions made using Earth models in which the viscosity above 1200 km depth is constrained to be 10^{21} Pa s, do not exhibit the multiple solutions characteristic of the $\nu_{UM} = 10^{21}$ Pa s calculations. The same is true of Earth models in which the upper mantle viscosity is weakened an order of magnitude to 10^{20} Pa s. The theory described herein is also applied to compute the $\dot{J}_\ell$ signal ($\ell \leq 10$) arising from the retreat of small ice sheets and glaciers described by Meier (1984) and also from any potential variations in the mass of the Antarctic and Greenland ice sheets. The present day $\dot{J}_\ell$ signal due to the late Pleistocene glacial cycles dominates the signal from Meier's sources at all degrees except ℓ=3. In contrast, the $\dot{J}_\ell$ signal arising from mass variations in the Antarctic and Greenland ice sheets is potentially comparable to the former. A comparison of observational constraints on the $\dot{J}_\ell$ data with predictions of the postglacial rebound signal described in this paper, in order to infer mantle rheology, cannot proceed until constraints are placed on the present-day mass flux of these large polar ice sheets. We show that the constraints required are weakest at degrees ℓ=2 and 4. Finally, we outline a potentially important procedure for incorporating predictions of the $\dot{J}_\ell$ signal due to the late Pleistocene glacial cycles and Meier's sources, with an observational constraint on the $\dot{J}_2$ datum, to yield bounds on the present-day net mass flux from the Antarctic and Greenland ice sheets. A rigorous application of this procedure must wait until observational constraints on $\dot{J}_2$ are reestablished in the literature.

[1]Now at Department of Physics, University of Toronto, Toronto, Ontario, Canada.

Paper number 92JB02700.
0148-0227/93/92JB-02700$05.00

INTRODUCTION

Satellite-derived maps of Earth's geoid reveal a field of marked complexity [e.g., *Marsh et al.*, 1990]. At the largest wavelengths the geoid undulations are dominated by the signal from the convective circulation in Earth's interior [*Richards* and *Hager*, 1984; *Forte and Peltier*, 1987, 1991; *Ricard and Vigny*, 1989];

however, a multitude of other effects also contribute [*Richards and Hager*, 1988]. This paper is concerned with the influence on the geoid of two phenomena: first, the present-day isostatic disequilibrium associated with incomplete adjustment following the last major late Pleistocene deglaciation event of the current ice age; second, the present-day retreat of small ice sheets and glaciers [*Meier*, 1984] and any recent variations in the mass of the Antarctic and Greenland ice sheets.

In previous work the late Pleistocene deglaciation induced anomaly in Earth's gravitational field has been isolated from other contributors to that field using two approaches. First, peak geoid and/or free-air gravity anomalies over previously glaciated regions have been considered [e.g., *Wu and Peltier*, 1983; *Mitrovica and Peltier*, 1989]. Recent work, however, has suggested that even when such regions coincide with apparently stable continental cratons (as, for example, in Laurentia), the signal associated with the mantle convective circulation may still constitute the dominant contribution to the observed anomaly [*Peltier et al.*, 1991, 1992]. An alternate approach to isolating the anomaly due to incomplete glacial isostatic adjustment, given the relatively short relaxation time associated with this process, is to consider secular variations in Earth's gravity field [*Wu and Peltier*, 1984; *Yoder and Ivins*, 1985; *Peltier et al.*, 1986; *Mitrovica and Peltier*, 1989]. Continuing advances in absolute gravity instrumentation [*Zumberge et al.*, 1982] will make it possible to accurately determine local values of $\dot{g}$, associated with glacial isostatic adjustment, within the next decade [*Mitrovica and Peltier*, 1989]. Furthermore, global measures of the secular variation in Earth's geopotential can be obtained through an analysis of satellite ranging data. Of particular interest are the amplitudes of the zonal harmonics in the spherical harmonic decomposition of this variation, the so-called $\dot{J}_\ell$.

A large number of studies have compared published values of the $\dot{J}_\ell$ coefficients, for $\ell \leq 4$ [e.g., *Peltier*, 1982, 1983; *Yoder et al.*, 1983; *Rubincam*, 1984; *Cheng et al.*, 1989] with predictions based upon numerical models of the glacial isostatic adjustment process, to derive constraints on the radial variation of mantle rheology [e.g., *Wu and Peltier*, 1984; *Peltier*, 1985; *Yoder and Ivins*, 1985; *Yuen and Sabadini*, 1985; *Yuen et al.*, 1987; *Mitrovica and Peltier*, 1989]. However, the value of $\dot{J}_2$ estimated from satellite ranging data is now under review (Eanes, personal comm.). It appears that the effect on the $\dot{J}_2$ estimate of the uncertainty associated with the J_2 signal from either the 18.6 year body tide (in particular, the influence of mantle anelasticity on this tide) or from slightly shorter time scale (5 to 12 years) phenomena (e.g. atmospheric pressure effects) has been underestimated. Fortunately, the extension of the LAGEOS (or Starlette) derived time series to encompass a full 18.6 year period (in approximately 4 years) should do much to decorrelate the $\dot{J}_2$ estimate from the effects of these phenomena. Furthermore, over the same time span, it will become possible to constrain the amplitude of the 18.6 year body tide using the available VLBI data set [*Herring*, 1986; *Davis et al.*, 1991].

The significance of estimates of the $\dot{J}_\ell$ coefficients extends beyond the inference of the radial viscosity profile in Earth's mantle. Recent analyses [*Yoder and Ivins*, 1985; *Peltier*, 1988; *Sabadini et al.*, 1988; *Trupin et al.*, 1992] have indicated that the present-day melting of small ice sheets and glaciers [e.g., *Meier*, 1984], as well as ongoing variations in the mass balance of larger ice sheets may have a non-negligible influence on present-day variations in Earth's geopotential. As a consequence, once estimates of the $\dot{J}_\ell$ coefficients are re-established, it may be possible to derive constraints on both mantle rheology and the extent of any present-day eustatic sea level rise that may also be occurring [*Peltier and Tushingham*, 1989].

These important applications require that the contribution to the $\dot{J}_\ell$ coefficients from both the present-day adjustment associated with the late Pleistocene glaciation history, and from any recent variations in the global ice/ocean mass balance, be determined as accurately as possible.

Previous numerical predictions of the late Pleistocene deglaciation induced signal in the $\dot{J}_\ell$ harmonics have adopted a number of approximations. The most significant of these relates to simplifications in the assumed space and time geometry of the late Pleistocene ice sheets. In the last 900 kyr these ice sheets have experienced a series of glacial cycles, each with a period of approximately 100 kyr [*Shackleton et al.*, 1990]. Numerical analyses [e.g. *Mitrovica and Peltier*, 1991*a*] have shown that predictions of the present day state of glacial isostatic disequilibrium and adjustment are most sensitive to the details of the disintegration pattern during the last major deglaciation, which extended from about 20 kyr to 5 kyr before present (B.P.). Previous numerical predictions of the $\dot{J}_\ell$ have, in general, ignored the complexity of this deglaciation event, and modelled each major ice sheet as a single circular, or elliptical, disc load with, most commonly, a fixed perimeter and drastically simplified mass loss history [see for example *Wu and Peltier* 1984; *Yuen et al.*, 1987 and *Mitrovica and Peltier*, 1989]. In addition, most studies have included, at most, only the largest of the late Pleistocene ice sheets (the Laurentide, Fennoscandian, and Antarctic ice sheets) in their analysis.

The growth and ablation of the ice sheets is, of course, fed by a complementary variation in the mass of the oceans. This variation constitutes a second significant component of the total surface load. Since the ocean loading perturbs the gravitational field of the planet (as a consequence of both its direct mass attraction, and the deformation of the solid planet which it produces), and is in turn governed by this field, the determination of a gravitationally self-consistent space and time variation of the ocean mass requires the solution of an integral equation known as the sea level equation [e.g., *Peltier and Andrews*, 1976]. To avoid this complication numerical predictions of the $\dot{J}_\ell$ harmonics have either ignored the ocean loading component entirely, or assumed that the meltwater enters or leaves the oceans eustatically (that is, independent of geography). One might easily assume that the latter approximation would be quite accurate. However, since the last major deglaciation event ended about 5 kyr B.P. the approximation implies no change in ocean bathymetry in the subsequent time interval. Gravitationally self-consistent calculations of ocean redistributions [e.g., *Clark et al.*, 1978; *Peltier et al.*, 1978; *Peltier and Tushingham*, 1989; *Mitrovica and Peltier*, 1991*b*] have, in contrast, shown that appreciable variations in ocean bathymetry, in response to the last major deglaciation event, have persisted to the present. It should not be too surprising if such variations were particularly efficient at exciting present-day variations in the zonal harmonics of Earth's geopotential.

In this paper we outline a new formalism for the prediction of secular variations in the spherical harmonic coefficients of the gravitational potential induced by space and time varying surface loads on a spherically symmetric, self-gravitating, viscoelastic planet. The theory allows for the input of a totally arbitrary ice loading history and incorporates a gravitationally self-consistent determination of the ocean mass redistribution component of the total surface load.

We use the new theory to examine the excitation of the $\dot{J}_\ell$ coefficients arising from the ongoing response of Earth to the late Pleistocene glacial cycles. In this respect we have three goals. First, to provide updated predictions of the coefficients using the recently constructed and highly resolved ICE-3G ice sheet model of the last major late Pleistocene deglaciation event [*Tushingham and Peltier*, 1991]. Second, to assess the sensitivity of the calculations to approximations made in previous analyses; in particular, in regards to the treatment of both the ice and ocean components of the surface load. Finally, we will use the results, together with determinations of Fréchet kernels (see below), to provide a rigorous assessment of the sensitivity of the $\dot{J}_\ell$ predictions to mantle rheology.

Predictions of the secular variations in the zonal harmonics due to the late Pleistocene glacial cycles have generally been limited to Earth models with an upper mantle viscosity of 10^{21} Pa s (as inferred by *Haskell* [1936] in his analysis of Fennoscandian uplift data), and an isoviscous lower mantle region with a viscosity value that serves as the free parameter of the analysis. Within this framework it is impossible to assess the detailed radial variations in the sensitivity of the $\dot{J}_\ell$ data to mantle rheology. In developing a formalism for the geophysical inversion of post-glacial rebound data *Mitrovica and Peltier* [1991*c*] derived expressions for Fréchet kernels for the $\dot{J}_\ell$ data. These (radially dependent) kernels map arbitrary perturbations in the radial viscosity profile of Earth model to variations in the data, and as such can be used to derive the true constraints on mantle rheology which the $\dot{J}_\ell$ data provide. *Mitrovica and Peltier* [1991*c*] found, for example, that the $\dot{J}_\ell$ ($\ell \leq 4$) data were most sensitive to viscosity variations at the very base of the mantle. Since the forward problem is a non-linear function of viscosity [*Peltier*, 1974], the Fréchet kernels will be a function of Earth model used for their derivation. *Mitrovica and Peltier* [1991*c*] used a model with a factor of two increase in viscosity across the 670 km boundary from an upper mantle value of 10^{21} Pa s. It is not clear how the detailed sensitivity of the $\dot{J}_\ell$ data, to the radial mantle viscosity profile, will be altered by a change in this Earth model.

The expressions for the Fréchet kernels derived by *Mitrovica and Peltier* [1991*c*] are valid only for a simplified saw-tooth ice loading history and a eustatic ocean loading component. We will use the new theory discussed above as a basis from which to derive Fréchet kernels associated with the $\dot{J}_\ell$ predictions which are valid for an arbitrary surface load history which includes a gravitationally self-consistent ocean mass redistribution. The technique for computing the Fréchet kernels described herein is, furthermore, applicable to any data set associated with the glacial isostatic adjustment phenomenon, and can be applied to any forward (or direct) theory for computing that adjustment.

We will compute Fréchet kernels for the $\dot{J}_\ell$ data using Earth models with widely varying mantle viscosities in order to examine the manner in which the detailed sensitivity of the $\dot{J}_\ell$ data, to variations in the mantle viscosity profile, may be altered. The analysis will be complemented by a suite of forward calculations which, for the first time in the context of $\dot{J}_\ell$ predictions, consider both the upper and lower mantle viscosities as free parameters.

A recent inversion of the relaxation spectrum derived from the post-glacial uplift of central Fennoscandia (*Mitrovica and Peltier* [1992], following *McConnell* [1968]) has yielded a set of rigorous constraints on the radial viscosity profile beneath that region. These constraints can not rule out an average upper mantle viscosity lower than the classical value of 10^{21} Pa s adopted from the work of *Haskell* [1986] (in fact, the constraint suggests that a lower band on ν_{UM} may be approximately 3 x 10^{20} Pa s if only McConnell's relaxation spectrum is employed as constraint). As a consequence, it is prudent to consider a parameter space which includes an appreciable variation in ν_{UM}.

In the final section of this paper we will consider the potential contribution to the present-day secular variations in the zonal harmonics $\dot{J}_\ell$ from recent meltings of smaller ice sheets and glaciers and from any mass variations which may be occurring in the much larger Antarctic and Greenland ice sheets. We will use the tabulation provided by *Meier* [1984] that formed the basis of the original analysis of *Peltier* [1988], which includes 31 glacial regions totalling approximately 0.38 mm/yr of eustatic sea level rise, as our model for the recent mass loss from smaller ice sheets and glaciers. Recent mass variations in the Antarctic and Greenland ice sheets are much more contentious, and our models for these events will consider the eustatic sea level change arising from each to be a free parameter. Since the Antarctic and Greenland continents cover very large geographic regions, the excitation of the $\dot{J}_\ell$ harmonics may be sensitive to the space dependence of any mass variations from the associated ice sheets. We will, accordingly, consider a variety of scenarios, including mass variations which are independent of position on the ice sheets, proportional to present day ice thickness, and limited to the perimeter of the ice sheets. All the calculations will incorporate a gravitationally self-consistent ocean loading component.

MATHEMATICAL FORMULATION

We begin by outlining the mathematical theory required for the forward calculations. The time domain impulse response of a spherically symmetric, self-gravitating, (Maxwell) viscoelastic planet can be written in terms of the spherical harmonic degree dependent surface load (viscoelastic) Love numbers defined by *Peltier* [1974]. These dimensionless numbers have the following forms:

$$h_\ell = h_\ell^E \, \delta(t) + \sum_{k=1}^{K} r_k^\ell \exp(-s_k^\ell t) \qquad (1a)$$

$$k_\ell = k_\ell^E \, \delta(t) + \sum_{k=1}^{K} r'^\ell_k \exp(-s_k^\ell t) \, . \qquad (1b)$$

The first term on the right-hand side of equations (1*a*) and (1*b*) represents the immediate elastic response (denoted by the superscript E) of the Earth model, and the second term is the nonelastic response. The latter is characterized by a finite multiplicity of modes of pure exponential decay, with amplitudes r_k^ℓ and r'^ℓ_k and inverse decay times s_k^ℓ. The Love numbers h_ℓ and k_ℓ represent the coefficients of degree ℓ in the Legendre polynomial expansion of the Green function for the (nondimensional) radial displacement and potential perturbation due to solid Earth mass redistribution, respectively. We use the formulation described by Peltier (1985) for the determination of those Love numbers.

The Green function for the geoid anomaly can be derived from equation (1*b*). It is [*Mitrovica and Peltier*, 1989]

$$GF_G(\gamma,t) = \sum_{\ell=o}^{\infty} \left\{ A_\ell \delta(t) + \sum_{k=1}^{K} B_k^\ell \exp(-s_k^\ell t) \right\} P_\ell(cos\gamma) \qquad (2)$$

where

$$A_\ell = \frac{a}{M_e} (1 + k_\ell^E) \qquad (3)$$

$$B_k^\ell = \frac{a}{M_e} r'^\ell_k \tag{4}$$

and the P_ℓ are Legendre polynomials. M_e and a represent the mass and mean radius of Earth, and γ is the angular distance from the observation point (say θ, ϕ) to the source point (θ', ϕ'). The appearance of the term equal to unity in equation (3) represents the contribution of the direct attraction of the point mass load on Earth's geopotential.

Let us now consider a general surface load $L(\theta, \phi, t)$. The response of the Earth model to such a load can be computed via a space-time convolution of the load history with the Green function (2). The result is

$$G(\theta,\phi,t) = \int_{-\infty}^{t} \iint_{\Omega} L(\theta',\phi',t')\, GF_G(\gamma, t-t')\, d\Omega'\, dt' + \xi(t) \tag{5}$$

where Ω represents the entire surface area of Earth. The term $\xi(t)$ is computed (see below) to ensure that the surface mass redistribution conserves mass.

As we have discussed, the surface load is often partitioned into the contributions from the ice and ocean loading. If $I(\theta, \phi, t)$ and $S(\theta, \phi, t)$ represent, respectively, the space-time history of the ice and ocean thickness, then we can write [*Peltier et al.*, 1978]

$$L(\theta,\phi,t) = \rho_I\, I(\theta,\phi,t) + \rho_w\, S(\theta,\phi,t) \tag{6}$$

where ρ_I and ρ_w are the densities of the ice and water, respectively. Since the late Pleistocene ice load reconstructions [e.g. *Tushingham and Peltier*, 1991] are often expressed in terms of a series of discrete melting episodes, it will be convenient to express the individual components of equation (6) in the form

$$I(\theta,\phi,t) = \sum_{n=1}^{N} H(t-t_n)\, \Delta I^n(\theta,\phi) \tag{7a}$$

$$S(\theta,\phi,t) = \sum_{n=1}^{N} H(t-t_n)\, \Delta S^n(\theta,\phi)\,. \tag{7b}$$

$H(t - t_n)$ is the Heaviside step function, and N is the total number of surface load increments. There is no loss of generality between equations (6) and (7) since the temporal discretization interval can, theoretically, be chosen arbitrarily small.

Since we will ultimately be concerned with secular variations in the harmonic amplitudes of Earth's geopotential, it will also be convenient to formulate the mathematics using a spherical harmonic approach. Accordingly, we consider the following spherical harmonic decompositions:

$$\Delta I^n(\theta,\phi) = \sum_{\ell=o}^{\infty} \sum_{m=-\ell}^{\ell} \Delta I^n_{\ell m}\, Y_{\ell m}(\theta,\phi) \tag{8a}$$

and

$$\Delta S^n(\theta,\phi) = \sum_{\ell=o}^{\infty} \sum_{m=-\ell}^{\ell} \Delta S^n_{\ell m}\, Y_{\ell m}(\theta,\phi) \tag{8b}$$

where the following normalization is employed for the surface spherical harmonics $Y_{\ell m}$:

$$\iint_{\substack{UNIT\\SPHERE}} Y_{\ell m}(\theta,\phi)\, Y^*_{\ell' m'}(\theta,\phi)\, \sin\theta\, d\theta\, d\phi = 4\pi\, \delta_{\ell\ell'}\, \delta_{mm'}\,. \tag{9}$$

Using equations (6), (7), (8) and (9), in equation (5) one can derive analytic expressions for both the space and time convolution [e.g., *Mitrovica and Peltier*, 1991*b*] and the result is

$$G(\theta,\phi,t) = \sum_{\ell=o}^{\infty} \sum_{m=-\ell}^{\ell} G_{\ell m}(t)\, Y_{\ell m}(\theta,\phi) \tag{10}$$

where

$$G_{\ell m}(t) = \frac{4\pi a^2}{(2\ell+1)} \Big[A_\ell (\rho_I I_{\ell m}(t) + \rho_w S_{\ell m}(t)) + \sum_{n=1}^{N} H(t-t_n) \sum_{k=1}^{K} \beta^\ell_k(t_n,t)\, (\rho_I \Delta I^n_{\ell m} + \rho_w \Delta S^n_{\ell m}) \Big] + \xi(t)\delta_{\ell o}\delta_{mo} \tag{11}$$

and

$$\beta^\ell_k(t_n,t) = \frac{B^\ell_k}{s^\ell_k} \left(1 - \exp(-s^\ell_k (t-t_n))\right). \tag{12}$$

$I_{\ell m}$ and $S_{\ell m}$ in equation (11) represent the spherical harmonic coefficients of the total ice and incremental ocean heights at time t. That is

$$I_{\ell m}(t) = \sum_{n=1}^{N} H(t-t_n)\, \Delta I^n_{\ell m} \tag{13a}$$

$$S_{\ell m}(t) = \sum_{n=1}^{N} H(t-t_n)\, \Delta S^n_{\ell m}\,. \tag{13b}$$

The secular variations in the spherical harmonic coefficients $G_{\ell m}$ can be determined, mathematically, by simply taking the time derivative of equation (11). In numerical applications of the theory, however, we have found it more convenient to compute the secular variations using the following simple second-order accurate, centered finite difference:

$$\dot{G}_{\ell m}(t) = \frac{1}{2\Delta t} \left\{ G_{\ell m}(t+\Delta t) - G_{\ell m}(t-\Delta t) \right\} \tag{14}$$

where $2\Delta t$ is chosen (in practise) to be a very small time interval (we have used $\Delta t = 5$ years).

The spherical harmonic coefficients of Earth's geopotential are generally defined using a different normalization than that expressed in equations (8) and (9) [*Garland*, 1979]. Indeed, in the case of the zonal harmonics J_ℓ, *Mitrovica and Peltier* [1989] have derived the following scaling factor:

$$\dot{J}_\ell(t) = -\frac{1}{a} (2\ell+1)^{1/2}\, \dot{G}_{\ell o}(t)\,. \tag{15}$$

The calculation of the coefficients $G_{\ell m}$, using equation (11), is complicated by the fact that the coefficients of the ocean height,

$S_{\ell m}(t)$, and the mass conservation term $\xi(t)$, are not known at the outset. In what follows we will very briefly outline the calculations involved in the determination of these terms. The interested reader is referred to *Mitrovica and Peltier* [1991*b*] for complete details. In analogy with equation (5), a Green function for the distance between the geoid and solid surface of the planet is given by

$$GF_s(\gamma, t) = \sum_{\ell=o}^{\infty} \left\{ C_\ell \, \delta(t) + \sum_{k=1}^{K} D_k^\ell \exp(-s_k^\ell t) \right\} P_\ell(\cos\gamma) \tag{16}$$

where

$$C_\ell = \frac{a}{M_e} \left(1 + k_\ell^E - h_\ell^E \right) \tag{17}$$

$$D_k^\ell = \frac{a}{M_e} \left(r'^\ell_k - r_k^\ell \right) . \tag{18}$$

This Green function is simply a scaled version of the potential perturbation Green function derived by *Peltier and Andrews* [1976].

Sea level variations can be determined by convolving the Green function (16) with the total surface load, yielding (using equation (6))

$$S(\theta,\phi,t) = C(\theta,\phi) \int_{-\infty}^{t} \iint_{\Omega} \left\{ \rho_I I(\theta',\phi',t') + \rho_w S(\theta',\phi',t') \right\} \cdot GF_s(\gamma, t-t') \, d\Omega' \, dt' + \xi(t) \tag{19}$$

where $C(\theta, \phi)$ is the ocean function, defined to be unity over the oceans and zero over the remaining surface of Earth. The term $\xi(t)$ can be determined by applying the conservation of mass constraint to the surface load. This yields (using equation 19)

$$\xi(t) = -\frac{1}{A_o} \left\langle \int_{-\infty}^{t} \iint_{\Omega} \left\{ \rho_I I(\theta',\phi',t') + \rho_w S(\theta',\phi',t') \right\} \cdot GF_s(\gamma, t-t') \, d\Omega' \, dt' \right\rangle - \frac{M_I(t)}{\rho_w A_o} \tag{20}$$

where A_o is the area of the oceans, $M_I(t)$ is the mass loss history of the ice sheets, and the symbol $< >$ denotes an integration over the ocean geography.

Equation (19) is an integral equation known as the sea level equation [e.g., *Peltier and Andrews*, 1976]. Its solution, under the constraint imposed by equation (20), will yield the sea level variations whose spherical harmonic coefficients are required as input to equation (11). *Peltier et al.*, [1978] developed a "finite element" approach to the solution of the sea level equation. More recently, *Mitrovica and Peltier* [1991*b*] have derived two spherical harmonic approaches to its solution, and we have adopted their 'pseudo-spectral' algorithm for the computations performed in the present study.

The theory described above can be used to determine the zonal harmonics in the secular variation of Earth's geopotential induced by arbitrary surface loads with gravitationally self-consistent mass redistributions. The necessity of solving the sea-level equation in this application can be avoided by making certain approximations for the ocean load variation. First, the ocean load can be ignored entirely, in which case the coefficients $\Delta S^n_{\ell m}$ and $S_{\ell m}$ may be set to zero in equation (11). A second approach is to assume that the ocean meltwater enters (or leaves) the oceans in a manner independent of geography. This is the so-called 'eustatic approximation', and it can be applied by replacing $\Delta S^n_{\ell m}$ and $S_{\ell m}$, in equation (11), by [e.g. *Mitrovica and Peltier*, 1991*b*]

$$\left\{ \Delta S^n_{\ell m} \right\}^{EU} = - \left\{ \frac{\rho_I}{\rho_w} \frac{4\pi a^2}{A_o} \Delta I^n_{oo} \right\} C_{\ell m} \tag{21a}$$

$$\left\{ S_{\ell m}(t) \right\}^{EU} = - \left\{ \frac{\rho_I}{\rho_w} \frac{4\pi a^2}{A_o} I_{oo}(t) \right\} C_{\ell m} \tag{21b}$$

where the $C_{\ell m}$ are the spherical harmonic coefficients in the expansion of the ocean function.

We turn now to a derivation of formulae for determining Fréchet kernels for the $\dot{J}_\ell$ data. The radially dependent Fréchet kernels relate arbitrary perturbations in the radial viscosity profile to the resulting variation in the data. One might proceed by taking the first variation (due to a radially dependent viscosity perturbation, which we denote by $\delta\nu(r)$) of the expression for the harmonics $\dot{J}_\ell$ in equation (15), and thus the $\dot{G}_{\ell o}(t)$ in equation (11). The terms dependent on the viscosity profile in equation (11) are the coefficients β_k^ℓ and the sea level harmonics $S_{\ell m}$ and $\Delta S^n_{\ell m}$. Thus $\delta\dot{G}_{\ell m}$ would be a function of $\delta\beta_k^\ell$, $\delta S_{\ell m}$ and $\delta\Delta S^n_{\ell m}$. *Mitrovica and Peltier* [1991*c*] proceeded in this manner and were obliged to assume that the sea level increments $\Delta S^n_{\ell m}$ (and thus $S_{\ell m}$) were stationary with respect to a perturbation in the viscosity profile. The $\delta\dot{J}_\ell$ were then a function of $\delta\beta_k^\ell$, and therefore, using equations (12) and (4), a function of the variation in each of the individual normal mode amplitudes and inverse decay times. *Peltier* [1976] derived a variational principle which permits the computation of radially dependent differential kernels which relate arbitrary perturbations in the radial viscosity profile to perturbations in the inverse decay times s_k^ℓ. *Mitrovica and Peltier* [1991*c*] have outlined a numerical approach which may be used to derive analogous kernels for the perturbation in the modal amplitudes r_k^ℓ and r'^ℓ_k. *Mitrovica and Peltier* [1991*c*] used both sets of kernels to complete the derivation for the Fréchet kernels relating $\delta\dot{J}_\ell$ to $\delta\nu(r)$.

The approach used by *Mitrovica and Peltier* [1991*c*] has the benefit of incorporating analytic results, but the disadvantage of requiring the stationarity of $S_{\ell m}$ and $\Delta S^n_{\ell m}$ with respect to a perturbation $\delta\nu(r)$. In the derivation which follows we will outline a completely numerical approach to determining the Fréchet kernels which is applicable to any data set related to the glacial isostatic adjustment phenomenon, and which does not suffer this limitation. It may also be applied, in principle, to any forward (or direct) theory for computing the adjustment of a planetary model.

Let us consider an arbitrary datum, χ, which is a non-linear function of the viscosity profile $\nu(r)$. We can define the Fréchet kernels for that datum, which we denote by $FK(\nu(r), r)$, through the following equation:

$$\delta\chi(\nu(r)) = \int_{CMB}^{a} r^2 \, FK(\nu(r), r) \, \delta log\, \nu(r) \, dr . \tag{22}$$

Peltier [1976] has derived an analytic expression which shows that the logarithm of the inverse decay times (S_k^ℓ) of the Earth model

scale with the logarithm of viscosity. Mitrovica and Peltier [1991c] have demonstrated, using numerical tests, that an analogous scaling holds for the modal amplitudes (r_k^{ℓ}, $r_k'^{\ell}$). The form of equation (22) is chosen accordingly.

If two forward calculations are performed using Earth models with viscosity profiles $\nu(r) + \delta\nu(r)$ and $\nu(r)$ (where $\delta\nu(r) << \nu(r)$), then, using equation (22), we can write

$$\chi(\nu(r) + \delta\nu(r)) - \chi(\nu(r)) \simeq \int_{CMB}^{a} r^2 FK(\nu(r), r) \cdot \log\left(1 + \frac{\delta\nu(r)}{\nu(r)}\right) dr \,. \tag{23}$$

if we choose

$$\xi(r - r_o) = \log\left(1 + \frac{\delta\nu(r)}{\nu(r)}\right) \tag{24}$$

to be a spatially localized (delta-like) function peaked at $r=r_o$ then we can make the approximation

$$FK(\nu(r), r_o) \simeq \frac{\chi(\nu(r) + \delta\nu(r)) - \chi(\nu(r))}{\int_{CMB}^{a} r^2 \xi(r - r_o)\, dr} \,. \tag{25}$$

The numerical procedure defined by equations (24) and (25) is identical to that described by *Mitrovica and Peltier* [1991c]; however in this case we have used it to derive the Fréchet kernels for each datum directly rather than for each of the normal mode amplitudes. The approach has the benefit of requiring no approximation beyond those incorporated into our forward analysis, and therefore it yields Fréchet kernels for the $\dot{J}_\ell$ datum (or any other datum related to the glacial isostatic adjustment process) which are valid for a spherically symmetric self gravitating viscoelastic Earth with an arbitrary ice load and gravitationally self-consistent ocean mass redistribution.

We have found that a perturbation in viscosity $\delta\nu(r)$ which yields a hat function $\xi(r\text{-}r_o)$ with an amplitude of 0.1 provides robust estimates of the kernels at most target depths $r=r_o$ for most viscosity models $\nu(r)$. In this respect the kernels were computed for 32 different radial regions, 22 of which resided in the lower mantle (this represents a hat function width of approximately 100 km in the lower mantle, and 50 km in the upper mantle; the numerical code used in the impulse response forward calculation incorporated three times as many node points). Fréchet kernels derived for various viscosity models $\nu(r)$ will be presented below.

CONTRIBUTIONS TO THE $\dot{J}_\ell$ HARMONICS FROM LATE PLEISTOCENE GLACIAL CYCLES: PREDICTIONS AND SENSITIVITY ANALYSES

$\dot{J}_\ell$ Predictions: Surface Load Considerations

In this section we consider forward calculations, or predictions, of the present day secular variations of the zonal harmonics $\dot{J}_\ell$ due to the late Pleistocene glacial cycles. The Earth model used in the calculations will have a radial viscoelastic structure consisting of a 120 km thick elastic lithosphere, elastic constants and density profile given by the seismic model PREM [*Dziewonski and Anderson*, 1981], isoviscous regions in the upper and (generally) the lower mantle, and an inviscid core. The values of the viscosity in the upper and lower mantle regions (to be denoted by, respectively, ν_{UM} and ν_{LM}) will serve as the free parameters of the model.

The recently published ICE-3G reconstruction of *Tushingham and Peltier* [1991] will be used as the standard ice loading model for the last major Pleistocene deglaciation event. The ICE-3G model was derived on the basis of glacial geomorphological and geophysical constraints, and is characterized by 14 deglaciation increments (N = 14 in equation (7)), at 1 kyr time intervals, extending from a glacial maximum at 18 ka to a minimum at 5 ka, beyond which no further ice melting is assumed to occur. The model includes ice sheets over Laurentia, the Arctic, the Canadian Cordillera, Greenland, Fennoscandia, Siberia, as well as many other regions (e.g., the British Islands, the Barents and Kara Seas, Chile, etc.), and it accounts for about 117 m of the 120 m eustatic sea level rise independently deduced by *Chappell and Shackleton* [1986] on the basis of oxygen isotope data.

In order to incorporate the cyclical nature of ice sheet growth and ablation we have added a glaciation phase of period 90 kyr constructed by simply reversing the sign of the spherical harmonic coefficients of the deglaciation increments and spacing them appropriately in time preceding the last glacial maximum. We have, furthermore, included three such glacial cycles (although the most recent cycle accounts for over 98% of the present-day response). This is certainly an approximation to the ice loading history for the period prior to the last glacial maximum, however the present-day response is strongly dominated by the details of the final deglaciation events [*Mitrovica and Peltier*, 1991*a*], for which the ICE-3G reconstruction provides the best available model to date.

The solid lines on Figure 1 represent predictions of the present-day value of the harmonics $\dot{J}_\ell$ ($2 \le \ell \le 10$) computed using the above specified ice loading and Earth models and a gravitationally self-consistent ocean loading component. The upper mantle viscosity, ν_{UM}, is held fixed at 10^{21} Pa s in the calculations while ν_{LM} varies between 10^{21} Pa s and 10^{23} Pa s.

The curves generally exhibit a pronounced maximum for a lower mantle viscosity intermediate to the extreme values considered [see also *Peltier*, 1983]. The reason for this is straightforward. The last major deglaciation event was assumed to be completed by 5 ka in the ICE-3G reconstruction, and thus Earth models with weak lower mantle viscosities (e.g., $\nu_{LM} = 10^{21}$ Pa s), and therefore relatively short relaxation times, will have small present-day rates of adjustment since they will have nearly returned to isostatic disequilibrium. Earth models with high lower mantle viscosities (e.g., $\nu_{LM} = 10^{23}$ Pa s) will, as a consequence of their long relaxation times, exhibit slow adjustment at all stages in their response. Earth models with intermediate values of ν_{LM} will have relaxation times short enough to ensure significant rates of adjustment, but long enough that appreciable disequilibrium persists to the present day.

The maxima in the curves of Figure 1 (generally) trend toward lower values of ν_{LM} as the degree ℓ under consideration increases. The reason for this is that for a particular Earth model the characteristic decay time of the fundamental mode of viscous gravitational relaxation generally increases as the degree is increased (the trend continues to about $\ell = 20$ [*Peltier*, 1976]). Therefore, as we consider higher degrees, the particular relaxation time which produces a maximum in the present day response (as discussed above) will be characteristic of Earth models with incrementally lower values of ν_{LM}.

A final characteristic evident in Figure 1 is that the amplitude of the variation in the predictions (measured as a fraction of the minimum value), at a particular degree, diminishes with increasing degree (as an example the $\dot{J}_2$ and $\dot{J}_{10}$ data predictions vary by a factor of about 4 and 0.4, respectively). This is a manifestation of the decreasing sensitivity of the $\dot{J}_\ell$ data, with increasing spherical harmonic degree, to the rheology of the lower mantle. This varying sensitivity will be investigated more explicitly later, where we compute Fréchet kernels for the $\dot{J}_\ell$ data.

The solid lines on Figure 1 will serve as a basis for the comparisons to be discussed in the remainder of this section. As an example, the dashed lines on Figure 1 are results generated in the same manner as the solid except that a different ice loading history (which we denote as the "disk load" model) has been utilized. The disk load model is based on approximations described by *Mitrovica and Peltier* [1989] and [1991*a*]. *Mitrovica and Peltier* [1989, Table 1] approximated the geometries of the major ice sheets included in the ICE-3G reconstruction using a series of elliptical discs (one for each ice sheet) with fixed perimeter and parabolic height variation, each having a very simple linear (in time) volume fluctuation during the glaciation and deglaciation phases. We adopt this model except we relax the constraint of a fixed perimeter and assume instead that the same volume fluctuation is achieved by maintaining plastic equilibrium in the ice sheets (see *Mitrovica and Peltier* [1991*a*] for details). As before, three full glacial cycles were included in the calculations.

Although the disk load model was adopted from the ICE-3G reconstruction, the results of Figure 1 indicate that substantial inaccuracies result when predictions are made on the basis of the simplified ice disc model rather than the detailed space-time geometry of the ICE-3G reconstruction. This indicates that predictions of the $\dot{J}_\ell$ harmonics are sensitive to relatively small errors in the space and time geometry of the late Pleistocene deglaciation event. Furthermore, disk load approximations to this deglaciation event, used in all previous considerations of the $\dot{J}_\ell$

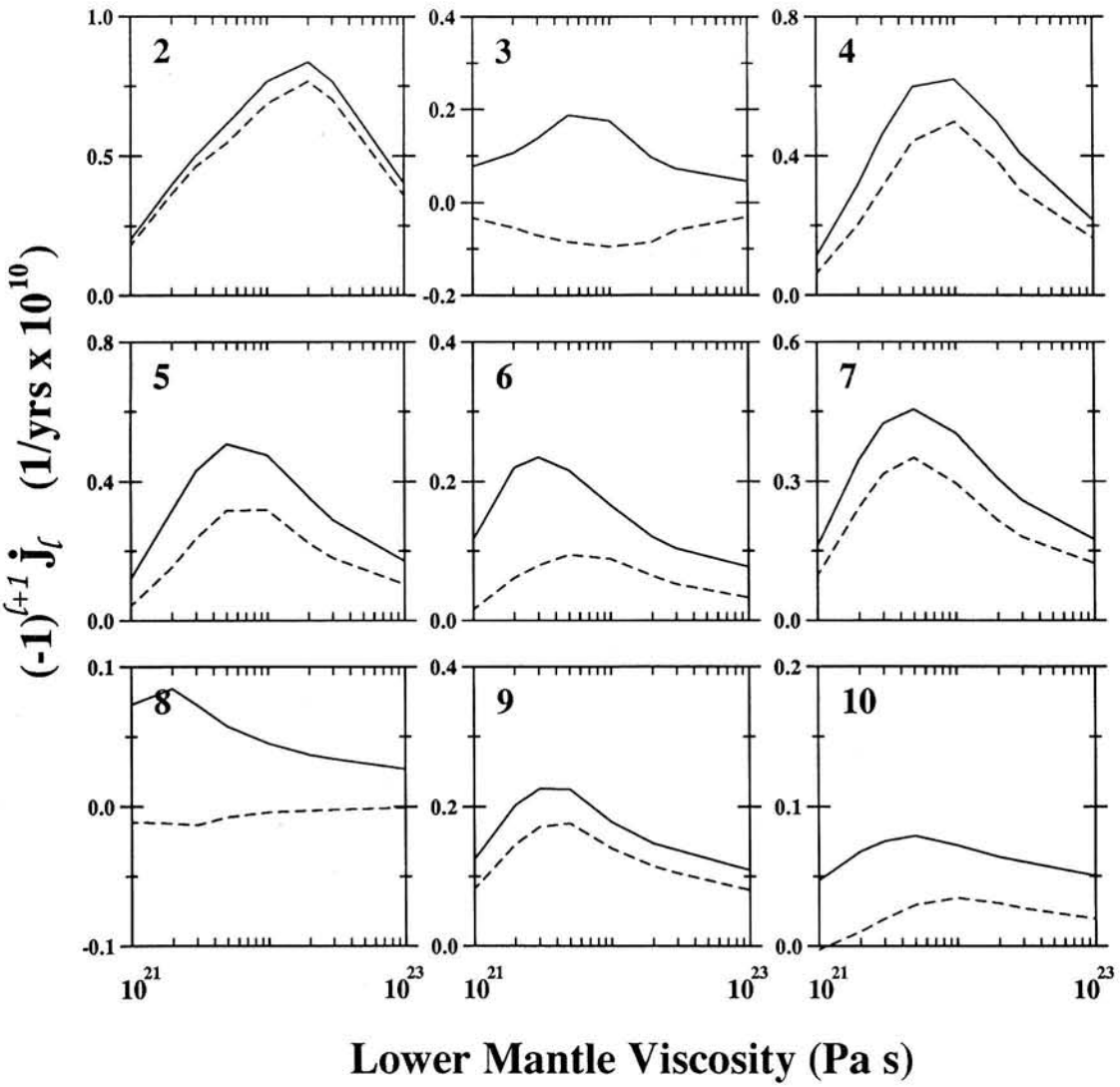

Fig. 1. Predictions of the zonal harmonics $\dot{J}_\ell$ (with the label on each frame referring to the spherical harmonic degree ℓ) computed using the Earth model discussed in the text with an isoviscous upper mantle viscosity of 10^{21} Pa s and a lower mantle viscosity ranging from 10^{21} to 10^{23} Pa s (as indicated by the abscissa). The solid and dashed lines refer to predictions using, respectively, the ICE-3G and disk load model described in the text. In each case three full glacial cycles are assumed in the analysis, and the ocean loading component of the surface load is computed using the gravitationally self-consistent theory.

harmonics, have yielded inaccurate predictions of these harmonics, and must be abandoned in favour of more detailed ice load reconstructions using the theory outlined previously.

Predictions of $\dot{J}_2$ are least sensitive to inaccuracies in the ice disk model, though even at this degree the errors are non-negligible (as high as order 10%). The P_2^0 Legendre polynomial is the same sign northward of 54.7 °N as it is southward of 54.7 °S and therefore the contributions to $\dot{J}_2$ from the disintegration of the individual late Pleistocene ice sheets reinforce each other. As a consequence $\dot{J}_2$ predictions will tend to be sensitive to errors in the total mass loss of the ice sheets, or alternatively errors in the total eustatic sea level rise attributed to the final late Pleistocene deglaciation event (as was shown by *Wu and Peltier* [1984]). The predictions are, of course, also sensitive to errors in the timing of the final deglaciation event. The ice disk model, since it exactly matches the total eustatic sea level rise associated with the ICE-3G deglaciation model, and closely approximates the chronology of that model, performs relatively better at degree 2 than at other degrees.

The results for $\dot{J}_3$ provide another important illustration of these arguments. During the last Pleistocene deglaciation event by far the most significant mass loss occurred in the Laurentian and Antarctic ice complexes [*Tushingham and Peltier*, 1991]. Since the P_3^0 Legendre polynomial is of opposite sign northward of 39°N than southward of 39°S, the contribution to $\dot{J}_3$ from the response associated with these ice sheets are of opposite sense. Indeed, detailed modelling (in the course of this study and by *Mitrovica and Peltier* [1989]) has shown that those contributions are relatively closely matched (notice the relatively small amplitude of the $\dot{J}_3$ prediction in comparison to the $\dot{J}_2$ and $\dot{J}_4$ predictions on Figure 1) and therefore the total predicted response is sensitive to the details of the Laurentian and Antarctic melting histories as well as the details of the mass loss from the many smaller ice sheets.

The discrepancy evident in the top-middle frame of Figure 1 is a consequence of this sensitivity. The mismatch between the present-day $\dot{J}_3$ response due to Laurentide and Antarctic melting is large enough to dominate the prediction based on the actual ICE-3G deglaciation history. In contrast, errors introduced using the simplified ice disc model lead to inaccurate predictions which are dominated by the response due to the melting of smaller northern latitude ice sheets.

As a final example, the computed $\dot{J}_4$ response is dominated by the adjustment due to the melting of the Antarctic ice sheet, since the major northern latitude late Pleistocene ice sheets were very near the node of the P_4^0 Legendre polynomial [*Mitrovica and Peltier*, 1989]. As a consequence, modelling the Antarctic ice sheet as a single circular or elliptical disk load is clearly inadequate, and has led, on Figure 1 (top-right frame), to errors varying from approximately 20-45%, depending on the lower mantle viscosity. Of course, incorporating the full details of the space and time geometry of the late Pleistocene ice sheets is also fundamentally important in predictions of the $\dot{J}_\ell$ response at higher degrees (Figure 1).

A second component of the total surface load is the ocean load. In Figure 2 we investigate the sensitivity of the predictions of $\dot{J}_\ell$ to various models of the ocean load component. The solid lines on Figure 2 are transferred from Figure 1 and represent predictions using the gravitationally self-consistent treatment of ocean mass redistributions. The dashed lines were computed using the eustatic ocean loading approximation, and the dotted lines were computed by neglecting the ocean loading entirely.

Discrepancies between the three lines of Figure 2 are a function of spherical harmonic degree. There are cases (ℓ = 3,5 and perhaps 6) where the eustatic approximation is satisfactory, and others (ℓ = 2,8 and 10) when the approximation is as poor as that which would result from neglecting the oceans entirely.

Given the historical importance of the $\dot{J}_2$ datum in inferences of mantle viscosity, the errors incurred by the eustatic approximation in predictions of $\dot{J}_2$ are particularly significant. The peak discrepancy between the solid and dashed lines is almost twice as large as the error bar quoted by (for example) *Rubincam* [1984] (0.57×10^{-11} yr^{-1}). With the passage of time, as the observational datum is reestablished and as errors in the datum diminish, numerical predictions of $\dot{J}_2$ must adopt a gravitationally self-consistent ocean loading calculation.

Present-day ocean mass redistributions due to ongoing glacial isostatic adjustment associated with the late Pleistocene glacial cycles have been extensively examined [e.g., *Clark et al.*, 1978; *Peltier*, 1988; *Peltier and Tushingham*, 1989; *Mitrovica and Peltier*, 1991*b*]. A characteristic of the mass redistribution, common to all gravitationally self-consistent solutions of the sea level equation, is a net flux of ocean water away from the equatorial regions. *Mitrovica and Peltier* [1991*b*] isolated the mechanism for this mass redistribution and have termed it "equatorial ocean syphoning." Regions of Earth which experienced substantial late Pleistocene deglaciation, such as Canada and the Antarctic, have a glacial forebulge at their perimeter which is presently subsiding. Since a large portion of the forebulges are situated in (relatively high latitude) oceanic regions, water flows into these regions (or is "syphoned" away from the equator) as the subsidence proceeds in order to maintain hydrostatic equilibrium. Significantly, the eustatic ocean loading approximation, which allows for no redistribution of water within the oceans, is incapable of modelling the syphoning process.

Clearly, the redistribution of ocean mass from the equator towards the glacial forebulges at high latitude will have a dominant degree 2 geometry. It is not surprising, therefore, that the discrepancies in the predictions of $\dot{J}_\ell$ on Figure 2 are largest at this degree. The sign of the discrepancy indicates that the mass redistribution within the oceans (and the solid Earth deformation associated with this mass redistribution) inherent to the gravitationally self-consistent calculation tends to reduce the oblateness of the geoid. This is precisely as one would expect given a movement of mass away from the equatorial regions.

An equivalent explanation for the sign of the discrepancy on the ℓ = 2 frame of Figure 2 can be made on the basis of Earth rotation considerations. *Wu and Peltier* [1984] have shown that variations in $\dot{J}_2$ are proportional to variations in the angular velocity of Earth. Using their scaling, the discrepancy on the first frame of Figure 2 implies that the ocean syphoning mechanism characteristic of the gravitationally self-consistent calculation acts to increase the rotation rate of the planet (or decrease the length of day). Indeed, the peak effect on Figure 2 (top-left frame) (which occurs for Earth models with values of ν_{LM} near 2.0×10^{22} Pa s) relates to a present-day decrease in the length of day of approximately 1.7×10^{-3} ms/yr. Once again, this is consistent with the reduction in the moment of inertia about Earth's rotation axis that would result from a transfer of mass away from the equatorial regions. The comparison of the predictions of $\dot{J}_2$ based on gravitationally self-consistent ocean loading calculations, and computations assuming an eustatic ocean redistribution, have thus isolated a heretofore unrecognized, and potentially significant, contribution to the long time scale non-tidal acceleration of Earth's axial rate of rotation (or, alternatively, secular variations in the degree 2 zonal term of Earth's geopotential).

As a final point, the strength of the ocean syphoning

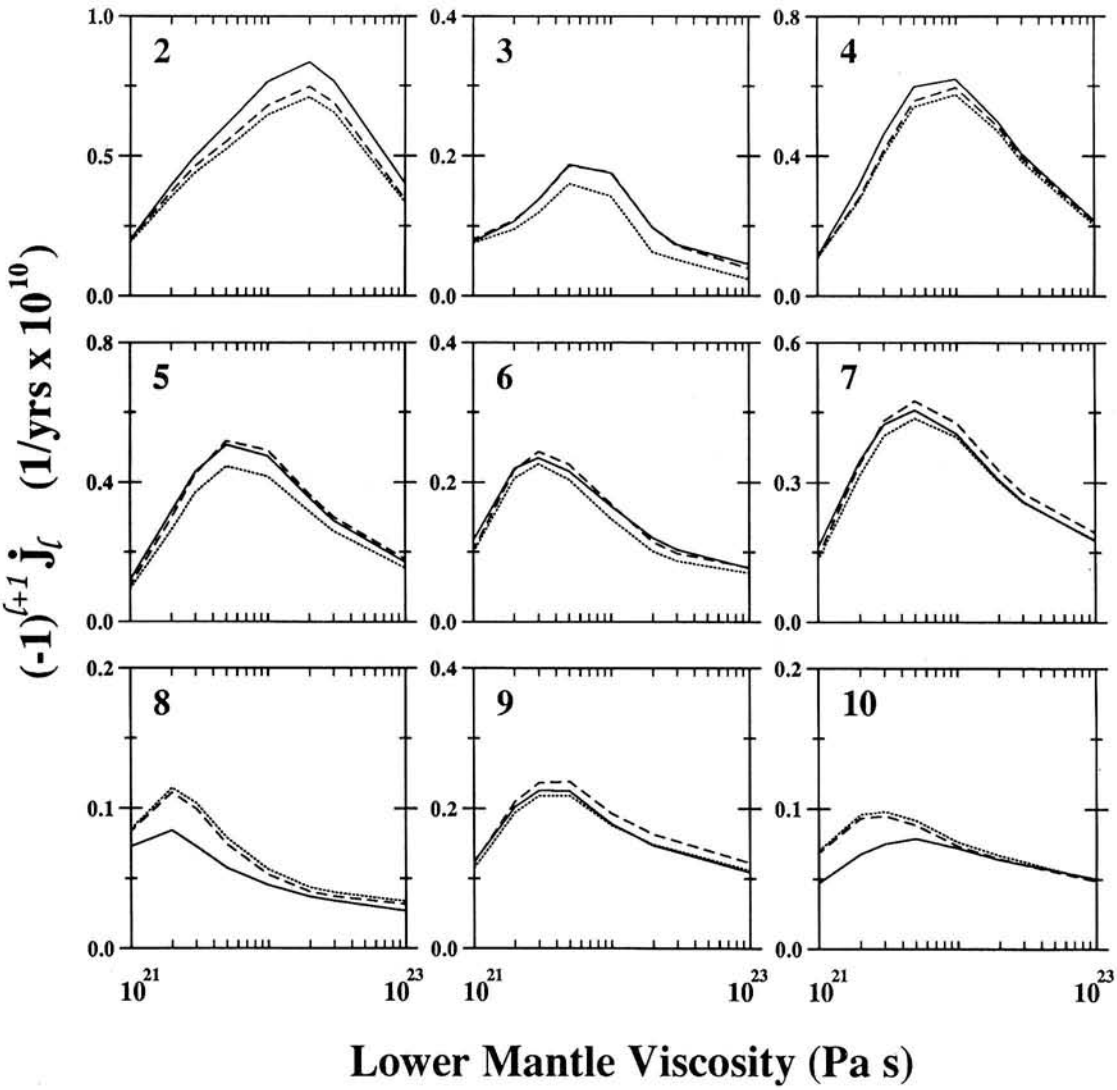

Fig. 2. Predictions of the zonal harmonics $\dot{J}_\ell$ (see Figure 1) using the ICE-3G deglaciation chronology of Tushingham and Peltier (1991a) modified to include three full glacial cycles. All calculations used $\nu_{UM} = 10^{21}$ Pa s. The three lines on each frame are distinguished according to the treatment of the ocean loading component. A gravitationally self-consistent calculation (solid line); application of the eustatic ocean loading approximation (dashed line); and the total neglect of an ocean load (dotted line).

mechanism, or alternatively the net flux of ocean water away from the equator, will be a function of the subsidence rate of the forebulge and therefore a function of the viscoelastic structure of the Earth model used in the calculations. Since $\dot{J}_2$ is a measure of the present day rate of glacial isostatic adjustment, it follows that the contribution to $\dot{J}_2$ from the ocean syphoning mechanism for a particular Earth model will be roughly proportional to the total predicted value of $\dot{J}_2$ for the same model. This is clearly the case on the degree 2 frame of Figure 2.

$\dot{J}_\ell$ Predictions: Sensitivity to Mantle Viscosity

In the last section we considered the sensitivity of the predictions of $\dot{J}_\ell$ to errors in the details of the surface mass load distribution (associated with the late Pleistocene glacial cycles) common to previous analyses. In this section we consider the sensitivity of the predictions to variations in the rheology of the mantle. All calculations will be performed using the ICE-3G deglaciation chronology and the gravitationally self-consistent ocean loading theory previously outlined. To begin, consider Figure 3, where the dotted lines refer to forward calculations of the $\dot{J}_\ell$ harmonics for Earth models with $\nu_{UM} = 10^{20}$ Pa s, or an order of magnitude less than the value used in the last section.

As discussed in the last section, calculations of the $\dot{J}_\ell$ harmonics, for Earth models with $\nu_{UM} = 10^{21}$ Pa s, are characterized by a pronounced peak over the range of ν_{LM} considered on Figure 3. Let us denote this peak as $\hat{\nu}^{\ell}_{LM}$. The relatively large slopes of the solid curve, evident on both sides of this peak value (particularly for $\ell \leq 7$), indicate that the $\dot{J}_\ell$ data ($\ell \leq 7$) are sensitive to lower mantle rheology for these classes of Earth models.

The results on Figure 3 suggest that reducing the upper mantle viscosity of the Earth model by an order of magnitude can have a profound effect on the sensitivity of the $\dot{J}_\ell$ datum to the rheology below 670 km depth. Indeed, with increasing spherical harmonic degree ℓ the computed (dotted) curves become progressively more flat for Earth models with $\nu_{LM} > \hat{\nu}^{\ell}_{LM}$ (and $\nu_{UM} = 10^{20}$ Pa s), indicating that flow is being confined more effectively to the upper mantle region. Furthermore, the amplitude of the computed present-day response for such Earth models ($\nu_{LM} > \nu^{\ell}_{LM}$) is

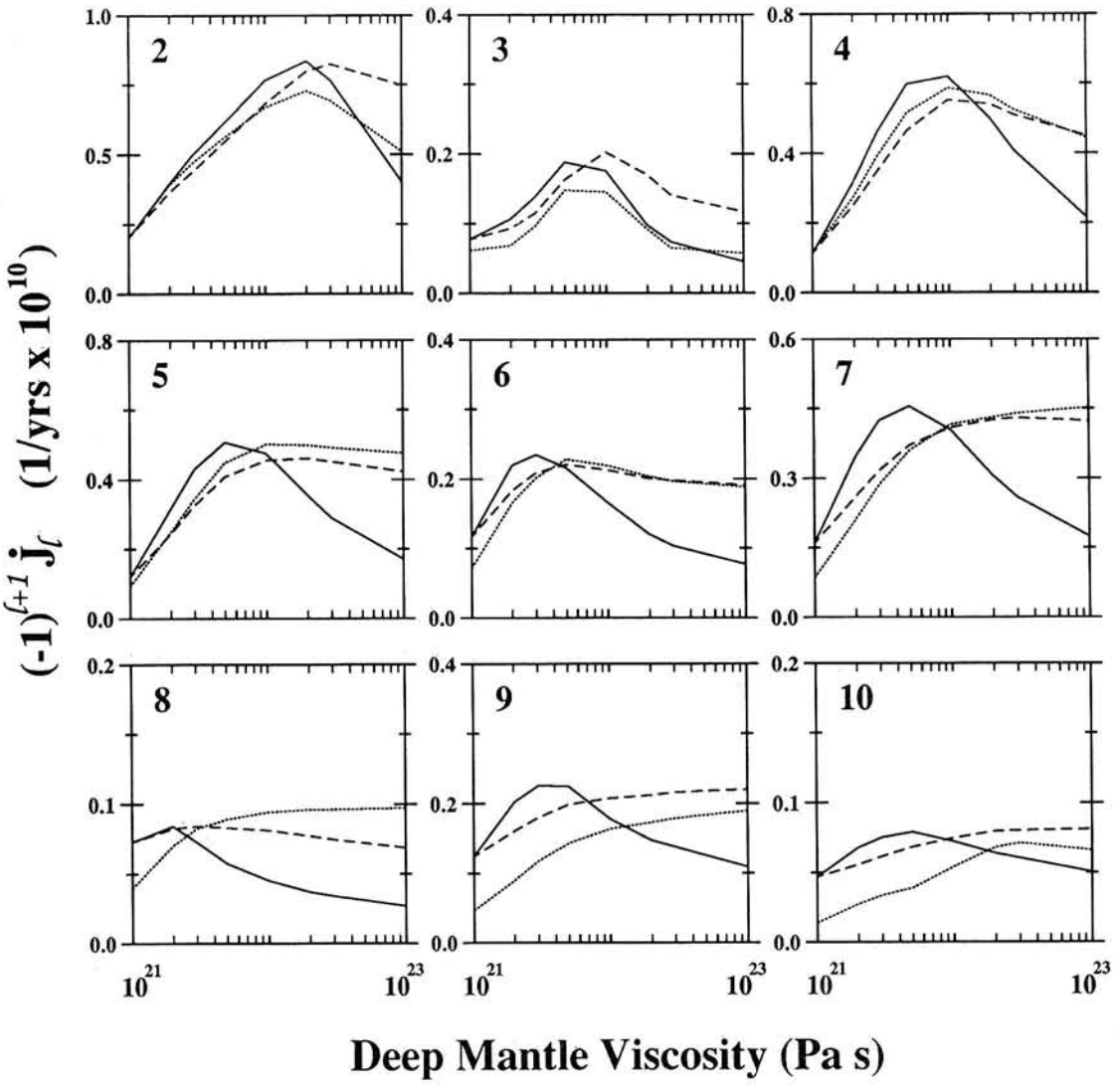

Fig. 3. Predictions of the zonal harmonics $\dot{J}_\ell$ (see Figure 1) using the ICE-3G deglaciation chronology modified to include 3 full glacial cycles. In all calculations the ocean loading component of the surface load is computed using the gravitationally self-consistent theory. The three lines on each frame are distinguished by the radial viscosity profile used in the calculation: ν_{UM} = 10^{21} Pa s; (solid line) ν_{UM} = 10^{20} Pa s (dotted line); and viscosity above 1200 km depth equal to 10^{21} Pa s (dashed line). The abscissa refers to the viscosity value of the Earth model below these respective regions.

appreciably higher, for the case ν_{UM} = 10^{20} Pa s, than that generated using Earth models with ν_{UM} = 10^{21} Pa s, suggesting that the characteristic relaxation time scale of the former set of models is short enough to yield appreciable rates of adjustment, while long enough to ensure that non-negligible disequilibrium persists. The result is that the potential ambiguity in inferences of ν_{LM}, which existed for Earth models with ν_{LM} = 10^{21} Pa s, is diminished considerably for the case of ν_{UM} = 10^{20} Pa s.

The sensitivity of the $\dot{J}_\ell$ data to lower mantle rheology diminishes with increasing degree ℓ. The sensitivity of the data to upper mantle rheology increases in the same sense. The latter is especially evident in the region $\nu_{LM} < \nu_{LM}^{\ell}$ on Figure 3, where the discrepancy between the solid and dotted curves becomes more pronounced as the degree ℓ rises.

It is of significance to note that the predictions for $\dot{J}_2$, though certainly sensitive to the order of magnitude reduction in ν_{UM}, retain a sensitivity to variations in lower mantle rheology over the full range of ν_{LM} considered on Figure 3. This indicates that appreciable degree 2 flow must persist below 670 km depth even in the case of Earth models with weak upper mantle rheologies and very large (> 2 orders of magnitude) viscosity stratification.

Inferences of mantle viscosity have come from geophysical observables related to both glacial isostatic adjustment [e.g., *Peltier*, 1974; *Cathles*, 1975; *Peltier and Andrews*, 1976] and the convective circulations in Earth's interior [e.g., *Richards and Hager*, 1984; *Forte and Peltier*, 1987; 1991]. There has been some suggestion in the latter class of analyses [*Forte and Peltier*, 1987] that Earth models with a viscosity jump at 1200 km, rather than 670 km depth, yield better fits to the appropriate data set (which include low-degree geoid undulations and plate motions). Accordingly, we have computed the $\dot{J}_\ell$ harmonics for Earth models with a viscosity of 10^{21} Pa s above 1200 km depth and a variable (isoviscous) value below it. The results are given by the dashed line on Figure 3, where the abscissa now denotes the viscosity below 1200 km depth.

The difference in the solid and dashed curves of Figure 3 is a

result of the difference in the viscosity of Earth models between 670 and 1200 km depth. Earth models with high deep mantle viscosities will tend to be characterized by a flow field which is relatively more confined to the region above the viscosity increase. It is not surprising, therefore, that the discrepancy between the solid and dashed curves is greatest for Earth models with very stiff deep mantle regions and that predictions of the $\dot{J}_\ell$ harmonics based on Earth models with a viscosity of 10^{21} Pa s between 670 and 1200 km depth exhibit larger amplitudes (i.e., shorter relaxation times) in this range of deep mantle viscosities. It is of interest to observe that the predictions for this class of Earth models (dashed lines, high deep mantle viscosity) are similar to those for Earth models with $\nu_{UM} = 10^{20}$ Pa s for $\ell > 3$. This suggests that at these degrees the relaxation times for Earth models in which flow is (approximately) confined to an upper mantle of viscosity of 10^{20} Pa s are comparable to those for Earth models in which the confinement occurs in a 1200 km region of viscosity 10^{21} Pa s.

As a final point, the small slope of the dashed curves on Figure 3, for Earth models with stiff deep mantle rheologies is, as before, a reflection of a gradual loss of sensitivity to the rheology in this region. This argues that the sensitivity to lower mantle viscosity evident on the solid curves of the same figure, for Earth models with $\nu_{LM} > \hat{\nu}^{\ell}_{LM}$, is due primarily to a sensitivity of the data to the rheology in the region between 670 and 1200 km depth. The result is that the ambiguity in inferences of deep mantle viscosity, which existed for Earth models with $\nu_{LM} = 10^{21}$ Pa s, essentially disappears for models with a viscosity of 10^{21} Pa s between 670 and 1200 km depth.

The forward calculations on Figure 3 provide only indirect evidence for the sensitivity of the $\dot{J}_\ell$ data to the radial mantle viscosity profile. A direct measure of the sensitivity requires the calculation of Fréchet kernels and in the remainder of this section we will consider kernels for the $\dot{J}_\ell$ data which have been computed (for various Earth models) using the theory previously outlined. As an example, the Fréchet kernels for degrees 2 through 10, for Earth model with $\nu_{UM} = 10^{21}$ Pa s and $\nu_{LM} = 3 \times 10^{21}$ Pa s, are given on Figure 4. (The discretization evident on the figure reflects the 32 radial regions in which the numerical prediction scheme outlined above is applied. (The kernels discussed in this section are all scaled by r^2 (see equation (22)) in order to facilitate a comparison of sensitivities at various depths.)

For this particular Earth model the $\dot{J}_\ell$ data, for $\ell \leq 5$, have a non-negligible sensitivity to variations in viscosity which extends to the deepest regions of the mantle. Indeed, the kernels for degrees 2 and 3 peak at the CMB. As the spherical harmonic degree is increased the peaks in the kernels tend to migrate to shallower regions of the mantle. This migration is accompanied by a reduction in the amplitude of the kernels within the lower mantle, reflecting a gradual loss of sensitivity of the data to the rheology of this region. This is, of course, manifested on Figure 3 by the gradual reduction in the slope of the solid lines at $\nu_{LM} = 3 \times 10^{21}$ Pa s (notice that the near-zero amplitude of the $\dot{J}_6$, $\dot{J}_9$ and $\dot{J}_{10}$ kernels in the lower mantle on Figure 4 is consistent with the fact that the solid lines on Figure 3 peak near $\nu_{LM} = 3 \times 10^{21}$ Pa s for the frames associated with these degrees).

Clearly the information provided by the Fréchet kernels is compelling, however it is incomplete unless one considers the dependence of the various sensitivities on the radial viscosity profile of Earth model used in the calculations. On Figure 5 we show Fréchet kernels for the $\dot{J}_2$ datum for Earth models with three different values of ν_{LM} (and $\nu_{UM} = 10^{21}$ Pa s; top frame) and two different values of ν_{UM} (with $\nu_{LM} = 3 \times 10^{21}$ Pa s; bottom frame).

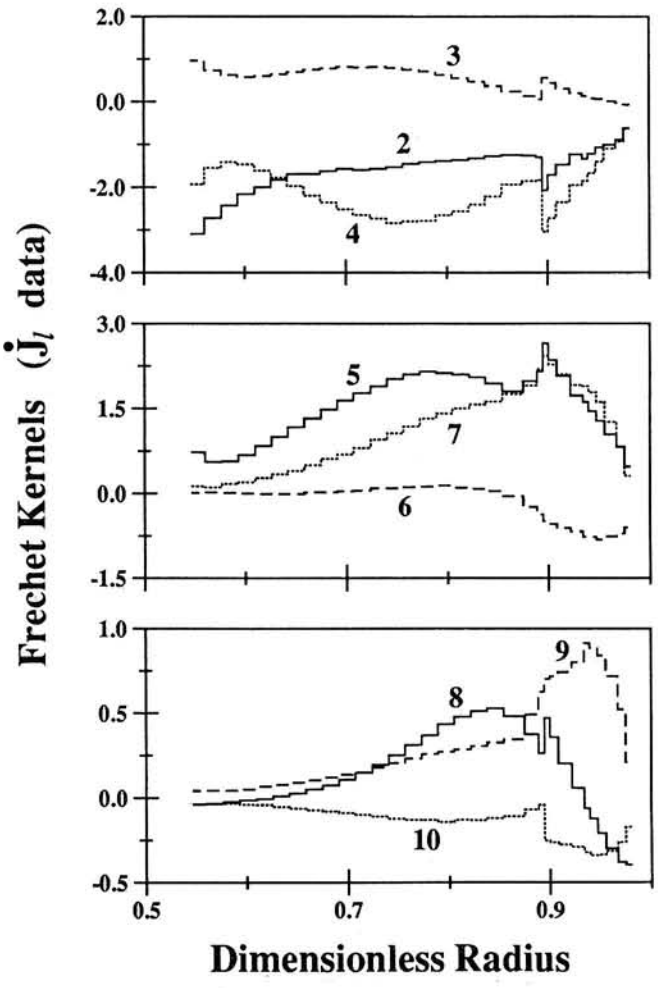

Fig. 4. Fréchet kernels for the $\dot{J}_\ell$ ($2 \leq \ell \leq 10$) data, as a function of radius (the abscissa is nondimensionalized using the mean radius of the Earth), computed using the ICE-3G deglaciation chronology (modified to include three full glacial cycles) and the standard Earth model described in the text with $\nu_{UM} = 10^{21}$ Pa s and $\nu_{LM} = 3 \times 10^{21}$ Pa s. The label on each kernel refers to the associated spherical harmonic degree ℓ. The kernels are scaled by a factor of 10^{10}.

The lower mantle viscosities considered on the top frame of Figure 5 span a range of ν_{LM} values which includes $\hat{\nu}^2_{LM}$ (approximately 2×10^{22} Pa s; Figure 3). Accordingly, the area under the curves varies from a negative value for the case of $\nu_{LM} = 3 \times 10^{21}$ Pa s (dotted line; reflecting the negative slope on Figure 3 for this Earth model at $\ell = 2$) to near zero for $\nu_{LM} = 2 \times 10^{22}$ Pa s $\approx \hat{\nu}^2_{LM}$ (solid line), and finally to a positive value for the high viscosity lower mantle model (dashed-line; a region of ν_{LM} space in which the forward predictions for $\ell = 2$ exhibit a positive slope).

The evolution of the kernels on Figure 5, as ν_{LM} is increased, is intriguing. As ν_{LM} approaches 2×10^{22} Pa s the sensitivity of the $\dot{J}_2$ datum to variations in rheology in the top 500 km of the lower mantle increases dramatically (to positive values). Surprisingly, the sensitivity of the datum to variations in rheology below this also increases, but much less dramatically and in the opposite sense. At $\hat{\nu}^2_{LM}$ the areas under the Fréchet kernel in the two regions CMB-1200 km depth and 1200 km - 670 km depth are equal and opposite, and the result is that the datum is stationary with respect to small perturbations in ν_{LM}.

As the lower mantle viscosity is increased from 2×10^{22} Pa s to

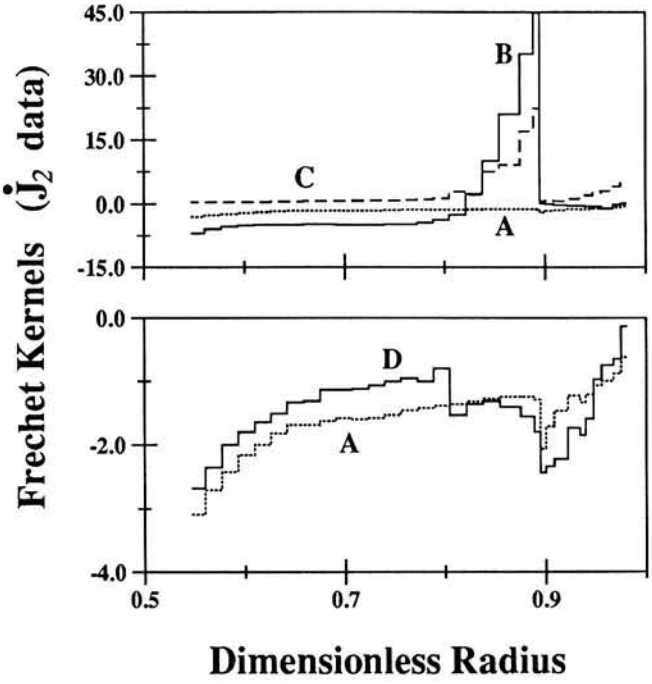

Fig. 5. Fréchet kernels for the $\dot{J}_2$ datum, as a function of dimensionless radius, computed using the ICE-3G deglaciation chronology modified to include three full glacial cycles. The Fréchet kernels on each frame are distinguished by the radial viscosity profile used in the calculations. If we specify a viscosity profile with isoviscous upper and lower mantle regions as (ν_{UM}, ν_{LM}), then the kernels labelled A, B, C and D were computed using the following profiles: A (10^{21} Pa s, 3 x 10^{21} Pa s); B (10^{21} Pa s, 2 x 10^{22} Pa s); C (10^{21} Pa s, 10^{23} Pa s); and D (3 x 10^{20} Pa s, 3 x 10^{21} Pa s). In each case the kernels are scaled by a factor of 10^{10}.

10^{23} Pa s the sensitivity of the $\dot{J}_2$ datum to variations in viscosity is diminished at all depths in the lower mantle. For an Earth model with $\nu_{LM} = 10^{23}$ Pa s the $\dot{J}_2$ datum is entirely insensitive to viscosity variations below about 1100 km depth, though an appreciable sensitivity to such variations persists in the 500 km region at the top of the lower mantle. We conclude that the two branches evident on the predictions for $\dot{J}_2$ on Figures 1 and 2 (and the solid lines on Figure 3), characteristic of Earth models with, respectively, a lower mantle viscosity less than and greater than $\hat{\nu}^2_{LM}$, reflect an evolution in the dominant sensitivity of the datum to viscosity variations in regions below approximately 1200 km depth to regions above this depth in the lower mantle.

The results for $\dot{J}_2$ on Figure 3 indicate that the second high viscosity branch disappeared when the viscosity in the region between 670 and 1200 km depth was constrained to be 10^{21} Pa s. The results on the top frame of Figure 5 indicate why this is the case. The slope of the second branch is due primarily to a sensitivity of the $\dot{J}_2$ datum to variations in viscosity between 1200 and 670 km depth, and therefore a set of Earth models which allow no viscosity variation in this region cannot manifest this sensitivity.

Over the entire range of lower mantle viscosities considered on the top frame of Figure 5 it is interesting to note that the $\dot{J}_2$ datum remains relatively (though certainly not entirely) insensitive to variations in upper mantle rheology. Not surprisingly, the greatest sensitivity to such variations is exhibited by Earth models with ν_{LM} = 10^{23} Pa s, though even in this case a constant perturbation in viscosity applied to the lower mantle will perturb the $\dot{J}_2$ datum approximately five times as much as an equal perturbation to the upper mantle viscosity. The Fréchet kernel for an Earth model with ν_{UM} = 3 x 10^{20} Pa s, given on the top frame of Figure 5, indicates that the depth-dependent sensitivity of the $\dot{J}_2$ datum to variations in the viscosity profile can be altered appreciably by weakening the upper mantle. In relation to the kernel for the case ν_{UM} = 10^{21} Pa s, a weakened upper mantle has reduced the sensitivity of the $\dot{J}_2$ datum to the rheology of the lower mantle below approximately 1250 km depth while increasing the sensitivity at shallower depths. For Earth model with ν_{UM} = 10^{21} Pa s (and ν_{LM} = 3 x 10^{21} Pa s) a small constant perturbation in the viscosity below 1250 km depth will perturb the $\dot{J}_2$ datum approximately two times as much as an equal perturbation to the viscosity above 1250 km depth. In contrast, similar perturbations to the Earth model with ν_{UM} = 3 x 10^{20} Pa s will have an almost equal effect on the datum (the ratio, in this case, is approximately 1.3:1).

On Figure 6 we show results analogous to Figure 5, for the case of ℓ=4. One difference in the figures is that the solid line on the top frame of that figure was computed using an Earth model with ν_{LM} = 7 x 10^{21} Pa s which is close to the value of $\hat{\nu}^4_{LM}$ evident on Figures 1-3. The conclusions drawn from Figure 5 are also applicable to the $\dot{J}_4$ case. One apparent difference is that the stationarity of the datum to variations in ν_{LM}, for Earth models with $\nu_{LM} \approx \hat{\nu}^4_{LM}$, is due not to a competing sensitivity at different regions to a constant lower mantle viscosity perturbation, but rather to a lack of sensitivity over the entire lower mantle (solid line, top frame of Figure 6). As ν_{LM} is increased above $\hat{\nu}^4_{LM}$, the high viscosity branch which occurs in the predictions (see Figures 1 and 2 and the solid line on Figure 3) is primarily a consequence of an emergent sensitivity of the datum to variations in the viscosity above 1000 depth. As in the case of the $\dot{J}_2$ datum, Earth models which constrain the viscosity of the shallow lower mantle region to a constant value will necessarily mask this sensitivity (see the dashed line on the top right frame of Figure 3).

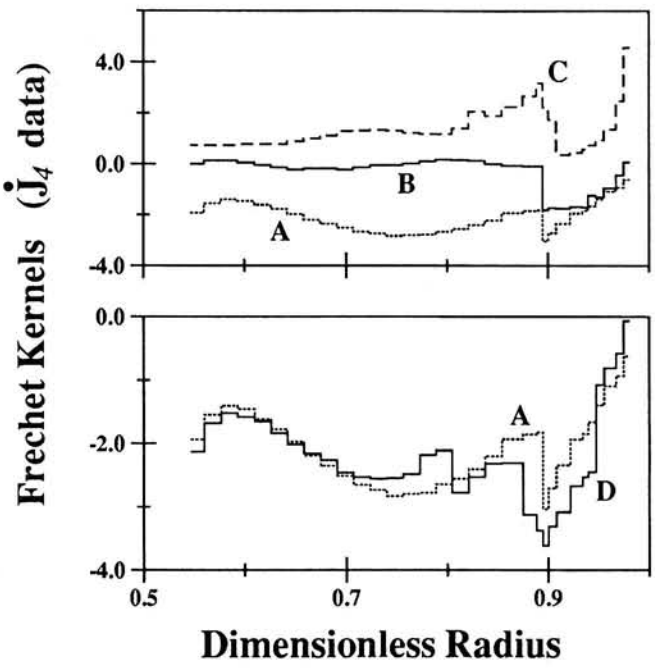

Fig. 6. As in Figure 5, except for the case of the $\dot{J}_4$ datum. The Earth models used in the calculation are as specified in Figure 5, except that the kernel labelled B (the solid line on the top frame) was computed using the viscosity profile (10^{21} Pa s, 7 x 10^{21} Pa s).

As a final point, as ν_{LM} is increased to very high values the sensitivity of the $\dot{J}_2$ and $\dot{J}_4$ data to variations in viscosity in the shallowest reaches of the lower mantle gradually diminishes. Forward predictions indicate that an Earth model with $\nu_{LM} = 10^{24}$ Pa s has very little sensitivity to viscosity variations in the lower mantle. It is interesting to note from the top frames of Figures 5 and 6 that the peak sensitivity of the $\dot{J}_2$ and $\dot{J}_4$ data to variations in upper mantle viscosity tends to migrate to shallower depths in the upper mantle as the lower mantle viscosity of Earth model is increased.

CONTRIBUTIONS TO THE $\dot{J}_\ell$ HARMONICS FROM CONTEMPORARY VARIATIONS IN THE GLOBAL ICE MASS

In this section we will consider the potential contribution to the zonal harmonics $\dot{J}_\ell$ from two sources. The first is the present-day retreat of 31 small mountain glaciers and ice sheets analyzed by *Meier* [1984], and the second is variations in the mass of the much larger Antarctic and Greenland ice sheets. All the calculations performed in this section will use the theory outlined previously for incorporating a gravitationally self-consistent ocean loading component in the total surface load.

The 31 sources included in *Meier's* [1984] analysis contribute a total of 0.38 mm/yr of equivalent eustatic sea level rise. In computing the individual contributions to this total we have used long-term mass balances wherever these are known [*Meier*, 1984]; in this respect, our ice model coincides with case II of *Peltier's* (1988, Table 1) tabulation of Meier's results. We have treated all sources as being spatially localized, point-like, masses.

The contribution to the $\dot{J}_\ell$ harmonics ($\ell \leq 10$) from Meier's sources is given on Figure 7, where the abscissa refers to the time from the onset of a continuous and constant melting episode. The results on the figure are in agreement with those computed previously by *Peltier* [1988] for $\ell = 2$ and by *Sabadini et al.* [1988] for $\ell \leq 10$. The very gentle slope in the curves on Figure 7 arises from a small non-elastic response over this time interval. Clearly the results are insensitive to assumptions regarding the viscosity profile of the Earth model.

A comparison of Figure 3 with Figure 7 indicates that the contribution to the $\dot{J}_\ell$ harmonics from ongoing glacial isostatic adjustment due to the late Pleistocene glacial cycles will dominate the signal due to Meier's sources at all degrees except ℓ=3, over the entire class of viscosity models considered on Figure 3. Indeed, between ℓ=4 and ℓ=8 the smallest $\dot{J}_\ell$ excitation on Figure 3 is at least an order of magnitude higher than the associated value on Figure 7.

It is interesting to note that the $\dot{J}_2$ signal contributed by Meier's sources (approximately 0.9×10^{-11} yr^{-1}) is almost identical in amplitude (and opposite in sign) to the maximum discrepancy between the gravitationally self-consistent and eustatic ocean loading calculations on the degree 2 frame of Figure 2. As we discussed above, this discrepancy is due to the ocean syphoning phenomenon [*Mitrovica and Peltier*, 1991b], which tends to move water away from the equatorial regions towards the peripheral bulges encircling the now vanished late Pleistocene ice sheets. Since most of Meier's sources are in high latitude regions, their net effect (that is, the total effect on the excitation of the P_2^0 polynomial) is in the opposite sense. Thus, just as the syphoning process reduces the oblateness of the geoid and the length of day, the effect of Meier's sources is to increase both (the latter by approximately 2×10^{-3} ms/yr, as previously demonstrated in *Peltier* [1988]).

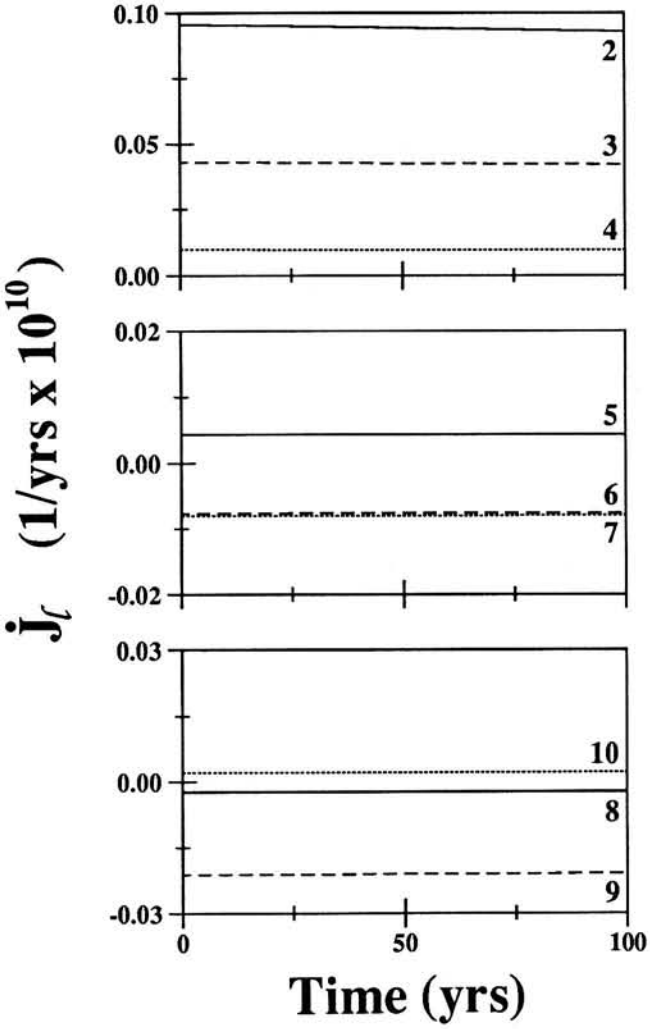

Fig. 7. Calculations of the contributions to the zonal harmonics $\dot{J}_\ell$ from the retreat of the 31 small ice sheets and glaciers described by Meier (1984). The net effect of the retreat is a eustatic sea level rise of approximately 0.38 mm/yr. The results are computed by assuming that this mass transfer is continuous, and the abscissa refers to the time from the onset of melting. The numerical label on each curve refers to the associated spherical harmonic degree ℓ. Calculations are performed using the Earth model described in the text with isoviscous upper and lower mantle viscosities of 10^{21} and 4.5×10^{21} Pa s, respectively.

Let us now consider the potential contribution to the $\dot{J}_\ell$ harmonics from mass variations in the Antarctic and Greenland ice sheets. *Peltier and Tushingham* [1989], in an analysis of global tide gauge records which they corrected for the influence of ongoing glacial isostatic adjustment, have inferred a present-day eustatic sea level rise of 2.4 ± 0.9 mm/yr. *Douglas* [1991], using the same approach but avoiding tide gauge records in areas of converging tectonic plates, has obtained an estimate of 1.8 ± .1 mm/yr. Using *Douglas'* [1991] estimate, and the total eustatic sea level rise of 0.38 mm/yr provided by Meier's sources, suggests that a sea level rise of approximately 1.4 ± 0.1 mm/yr is unaccounted for. Thermal expansion of the oceans [e.g., *Etkins and Epstein*, 1982] may account for a significant portion of this discrepancy (such variations will not contribute a $\dot{J}_\ell$ signal), however another potential source of sea level change is an ongoing net transfer of mass between the Antarctic and Greenland ice sheets and the global oceans. The contemporary mass balance of these polar ice

sheets is a subject of contention. As an example, there has been some suggestion that the Greenland ice sheet is in a growth phase [e.g., *Zwally*, 1989] and other suggestions of an opposite scenario [e.g., *Carter and Robertson*, 1990]. Given this uncertainty (which extends to mass variations of the Antarctic ice sheet), we will, in the calculations to be described in this section, consider the net mass variation in each of the ice sheets to be a free parameter. We will, in fact, assume a specific mass loss for the ice sheets (equivalent to a eustatic sea level rise of 1 mm/yr) with the understanding that the result can be scaled to yield predictions for any alternate scenario (including a growth of the particular ice sheet).

Since the Antarctic and Greenland ice sheets cover very large geographic areas, it is conceivable that the excitation of the $\dot{J}_\ell$ harmonics may be sensitive to the space-dependence of the mass variation on these ice sheets (see the analysis of Sabadini et al. (1988) for the case of the Antarctic ice sheet). We will, as a consequence, consider three different scenarios: First, that the mass flux occurs in a manner independent of geography on the ice sheets; second, that the mass flux is proportional to the present-day ice thickness; finally, that the mass flux occurs only on the perimeter of the ice sheets. The $\dot{J}_\ell$ excitation computed using these scenarios on the Antarctic and Greenland ice sheets are shown, respectively, on Figures 8 and 9. The abscissa refers to the time from the onset of a melting episode which raises equivalent sea level by 1 mm/yr.

The results of Figures 8 and 9 suggest that contemporary mass variations in the Antarctic and Greenland ice complexes are potentially very significant contributors to the present day secular variations in the zonal harmonics of Earth's geopotential. It is perhaps not generally appreciated that mass variations in the Greenland ice sheet are as efficient at exciting the secular

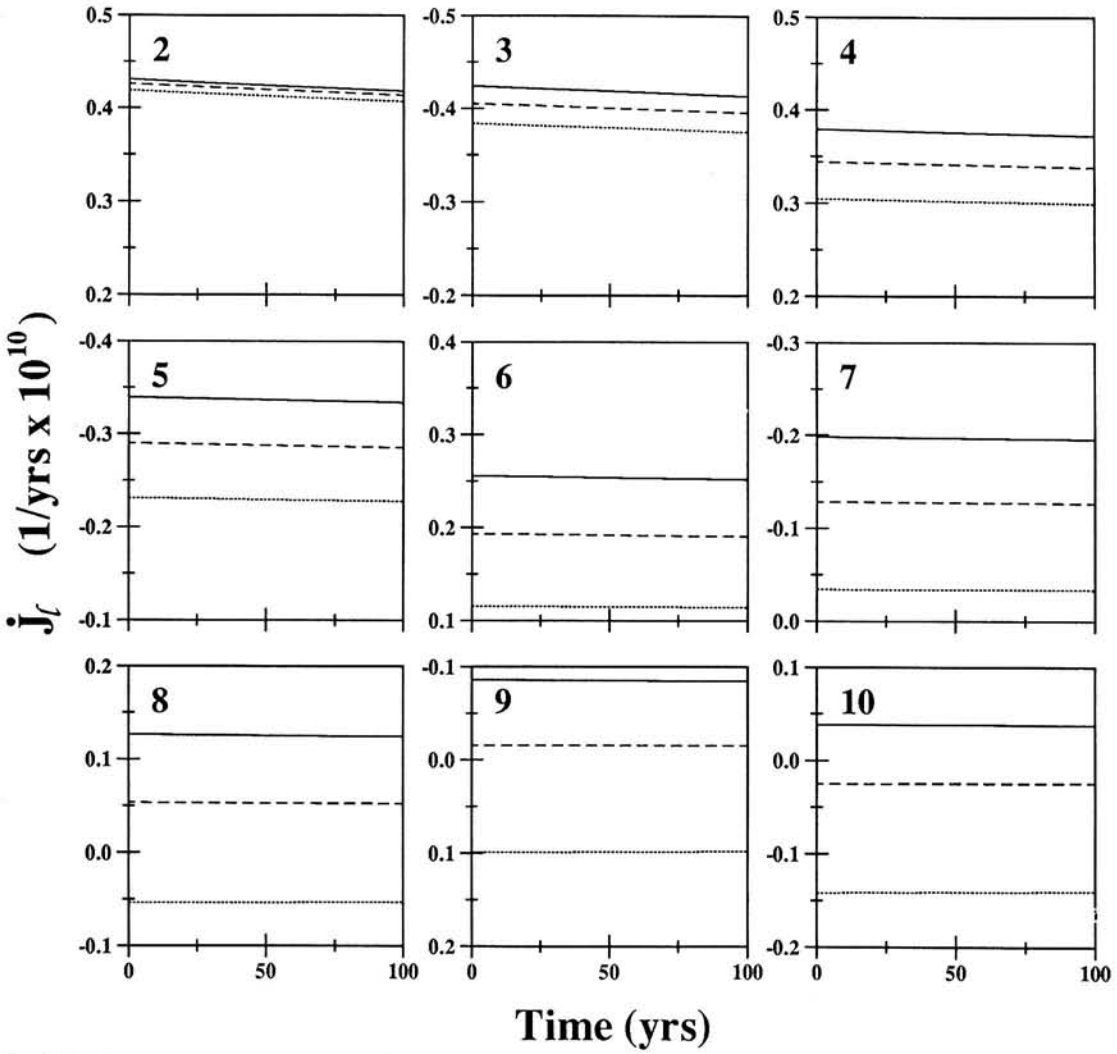

Fig. 8. Predictions of the zonal harmonics $\dot{J}_\ell$ (with the label on each frame referring to the spherical harmonic degree ℓ) as a function of time from the onset of continuous mass loss from the Antarctic ice sheet. Computations are performed assuming a mass loss equal to 1 mm/yr of eustatic sea level rise. The predictions for an alternate ice/ocean mass transfer (including a growth of the ice sheet) can be made by scaling the results on the figure accordingly. All calculations are performed assuming a gravitationally self-consistent ocean mass redistribution, and the three lines on each figure refer to different cases for the manner in which mass is removed from the Antarctic ice sheet: Solid line the mass variation is constrained to be proportional to the present day ice height; dashed line mass variation is constant over the entire ice sheet; dotted line mass variations occur only at the perimeter of the ice sheet. Calculations are performed using the Earth model described in the text with isoviscous upper and lower mantle viscosities of 10^{21} and 4.5×10^{21} Pa s, respectively.

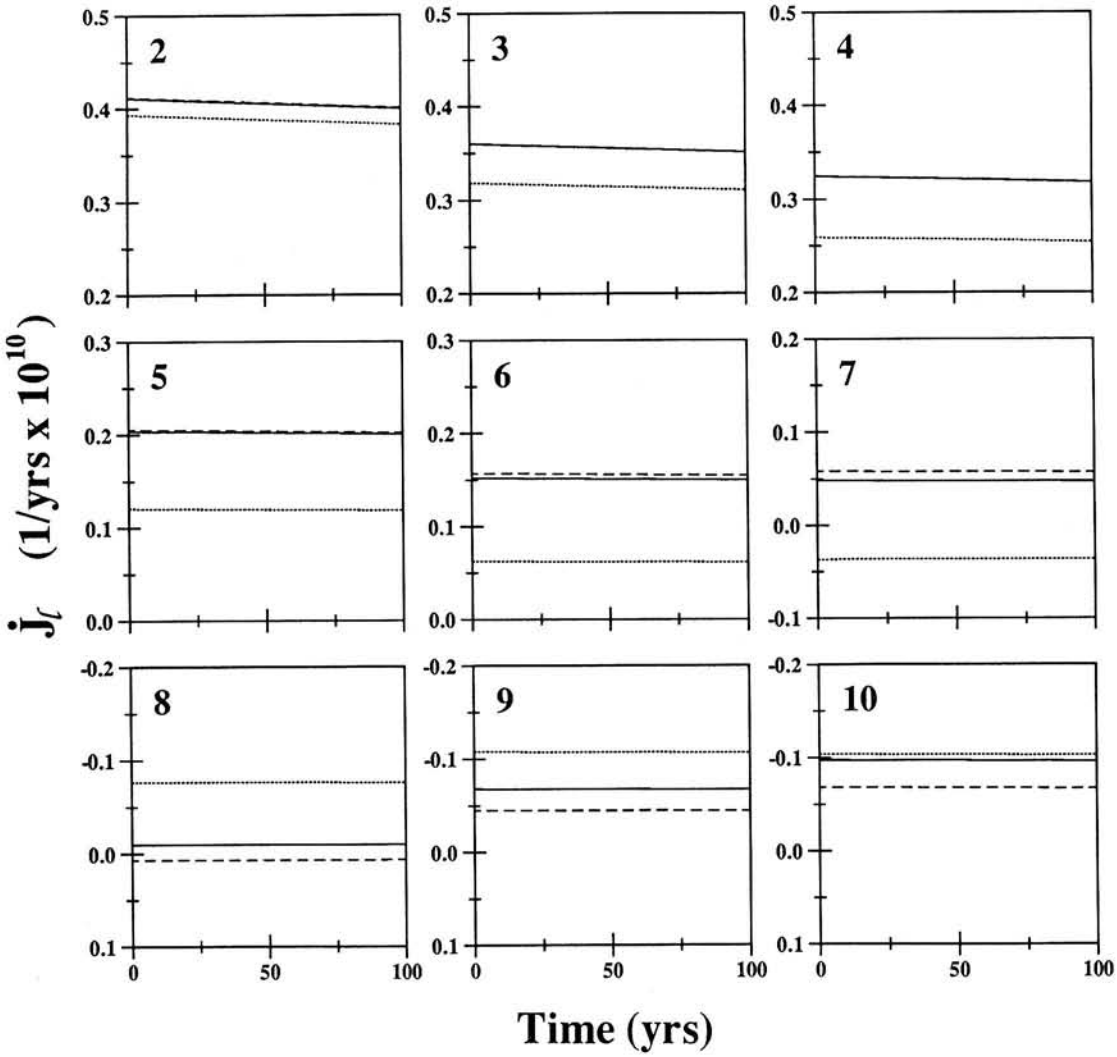

Fig. 9. As in Figure 8, except for the case of present-day mass variations on the Greenland ice sheet.

variations $\dot{J}_\ell$ as equal changes in the mass of the Antarctic ice sheet. A simple consideration of the $\dot{J}_2$ case indicates why this should be so. The center of the Greenland ice sheet is near 73°N latitude, while the center of the Antarctic ice sheet is near 82°S. The ratio of the P_2^0 polynomials evaluated at these latitudes is approximately 0.9 and thus mass variations on the Greenland ice sheet should be only about 10% less efficient at exciting a $\dot{J}_2$ response than mass variations on the Antarctic ice sheet. A comparison of Figures 8 and 9 indicates that this is indeed the case.

The results on Figures 8 and 9 also indicate, not surprisingly, that the $\dot{J}_\ell$ calculation generally becomes more sensitive to the assumed space-dependence of the mass variation as the spherical harmonic degree increases. Indeed, by degree 4 there is an order 30% variation between the predictions based on the three different cases treated on the figures. This indicates that an accurate prediction of the contribution of contemporary mass variations in the large polar ice sheets to the $\dot{J}_\ell$ harmonics, for $\ell \geq 4$, requires an accurate description of the spatial variation in the mass flux, and not simply an integrated measure of that variation (as is provided by the equivalent sea level change). It is important to note, however, that the predictions at degree 2, and to a slightly lesser extent degree 3, do not require such a detailed description.

The contributions to the $\dot{J}_\ell$ harmonics from the melting (or growth) of the Antarctic and Greenland ice sheets have the same sign at several degrees (e.g., ℓ=2, 4 and 6). This has important implications for the $\dot{J}_2$ harmonic in particular. Variations in the mass of the Antarctic and Greenland ice sheets are almost equally efficient at exciting a $\dot{J}_2$ response, and since the excitations are relatively insensitive to the spatial pattern of the mass variation, a very good approximation to the contribution to $\dot{J}_2$ from contemporary variations in the mass of those ice sheets requires only that the total contribution to the present-day eustatic sea level variation from these ice sheets be known. That is, one need not know how the Antarctic and Greenland ice sheets contribute independently to the eustatic sea level change (this holds whether the ice sheets grow or diminish in volume). As an example, if 1.0 mm/yr of eustatic sea level rise was occurring because of net changes in the mass balance of these polar ice sheets, then, from Figures 8 and 9, the contribution to the $\dot{J}_2$ harmonic due to this mass exchange (and, of course, the resulting response of the solid Earth) would be between 0.39×10^{-10} yr^{-1} and 0.42×10^{-10} yr^{-1}.

Whenever the excitation of the $\dot{J}_\ell$ harmonic is different for the Antarctic and Greenland ice sheet (given an identical mass flux, as in Figures 8 and 9), in amplitude and/or sign, the mass balance of each ice sheet must be known. This is a significant complication

to predictions of the contribution to the $\dot{J}_\ell$ harmonics, for $\ell > 2$, from mass variations in those polar ice sheets.

One of the fundamental results from Figures 8 and 9 is that variations in the mass balance of the larger polar ice sheets have the potential of exciting a $\dot{J}_\ell$ response which is comparable to the response arising from ongoing glacial isostatic adjustment (see Figure 3). This suggests that it is fruitless to attempt to constrain mantle rheology by comparing predictions of present day $\dot{J}_\ell$ harmonics of the kind described in the last section with any observational constraints, unless one can constrain variations in the mass of the Antarctic and Greenland ice sheets. Our results suggest that the response at ℓ=2, and to a lesser extent ℓ=4, may be most promising since it may be possible to consider only the net effect of mass variations from those ice sheets.

Finally, it is possible to use the results of this section and earlier results, together with observational constraints on the $\dot{J}_\ell$ data, to bound variations in the mass of the large polar ice sheets. Once again, the degree 2 case provides the most promising example. Figure 3 indicates that ongoing glacial isostatic adjustment may be reasonably expected to contribute a $\dot{J}_\ell$ excitation in the range -0.2 x 10^{-10} yr^{-1} to -0.8 x 10^{-10} yr^{-1}. Meier's sources provide a signal of approximately 0.1 x 10^{-10} yr^{-1} (Figure 7). Let us assume an observational constraint on $\dot{J}_2$ of -0.2 x 10^{-10} yr^{-1} to -0.32 x 10^{-10} yr^{-1} (this is the estimate quoted by Rubincam [1984]). The $\dot{J}_2$ contribution from mass variations in the Antarctic and Greenland ice sheets would therefore range from -.1 x 10^{-10} yr^{-1} to 0.5 x 10^{-10} yr^{-1} (this assumes that there are no other contributions to the $\dot{J}_2$ harmonic, however even a 50% error in the total contribution from the melting of small ice sheets and glaciers would not alter the results significantly). Using Figures 8 and 9, this suggests that the net mass balance on the Antarctic and Greenland ice sheets is contributing a eustatic sea level rise in the range -0.25 mm/yr to 1.25 mm/yr.

The main difficulty with this potentially important result is that the observational constraint on $\dot{J}_2$ is, as discussed in the introduction, now under review. If the estimate derived by *Rubincam* [1984] is revised, then the constraint on sea level rise will have to be altered accordingly. It is interesting to note, however, that the estimate derived by *Rubincam* [1984] agrees well with an independent constraint on the non-tidal acceleration of Earth derived by *Currot* [1966] from an analysis of ancient eclipse data [see *Wu and Peltier*, 1984].

Finally, an improvement in this procedure for constraining present-day eustatic sea level change due to a variation in the Antarctic and Greenland ice sheets is possible by invoking independent constraints on mantle rheology. Indeed, the 1.5 mm/yr range in the sea level constraint described above (which assumed the *Rubincam* [1984] estimate of $\dot{J}_2$) is due primarily to the range of predictions for $\dot{J}_2$ on Figure 3 arising from variations in the rheology of Earth model.

CONCLUSIONS

We have developed the mathematical formulation required for the prediction of secular variations in the geopotential for the case of a spherically symmetric, self-gravitating, (Maxwell) viscoelastic Earth model and an arbitrary surface load which can include a gravitationally self-consistent ocean loading component. In this paper the theory was specifically applied to predict the present-day secular variations in the zonal harmonics of the geopotential ($\dot{J}_\ell$, $\ell \leq 10$) arising from the surface mass loading associated with the late Pleistocene glacial cycles. In our opinion the results, which incorporate the very recent and well resolved ICE-3G reconstruction of the last late Pleistocene deglaciation event (Tushingham and Peltier, 1991), represent the most accurate prediction, to date, of this contribution.

In past analyses secular variations in the zonal harmonics have been computed by modeling a limited subset of the late Pleistocene ice sheets as ice disks with drastically simplified space-time geometries, and by assuming that meltwater enters the oceans eustatically. We have found that "ice disk" models introduce very large errors in the prediction of the $\dot{J}_\ell$ harmonics at all spherical harmonic degrees except ℓ=2, and conclude that such models should be abandoned in favour of realistic models of the late Pleistocene ice load geometry. A comparison of results obtained using the ICE-3G reconstruction and the ice disk model (which was constructed as an approximation to the ICE-3G model) indicates that the forward predictions can be sensitive to relatively small variations in the model of ice sheet collapse during the last late Pleistocene deglaciation event.

The accuracy of predictions of the $\dot{J}_\ell$ harmonics which assume a eustatic ocean loading component varies with spherical harmonic degree. We have found that the performance of the eustatic approximation at degrees 2, 8 and 10 is particularly poor, and characterized by an error which is comparable to that which results from neglecting the ocean loading component entirely. Given the historical importance of the $\dot{J}_\ell$ datum in inferences of mantle rheology, future calculations of these harmonics should incorporate the gravitationally self-consistent theory for ocean loading. The imminent measurement of the higher degree zonal harmonics from an analysis of long time series satellite ranging data also provides an impetus towards the more accurate theory.

A comparison of the predictions of $\dot{J}_2$ using the gravitationally self-consistent theory and the ocean loading approximation has isolated a heretofore unrecognized contribution to the datum (or alternatively a contribution to the non-tidal acceleration of Earth's axial rate of rotation). Gravitationally self-consistent determinations of present-day sea level variations due to the late Pleistocene glacial cycles have indicated a net flux of water away from the equatorial regions [*Clark et al.*, 1978; *Peltier* 1988; *Peltier and Tushingham* 1989, 1991; *Mitrovica and Peltier*, 1991*b*). *Mitrovica and Peltier* (1991*b*) have isolated the physical mechanism for this flux, which they associate with the subsidence of existing glacial forebulges, and have termed it "equatorial ocean syphoning". Calculations using the eustatic ocean loading approximation are incapable of modelling the syphoning process, and we have found that the error which results in the $\dot{J}_2$ prediction can be of order 10% of the total contribution from the late Pleistocene glacial cycles. The maximum discrepancy is approximately -10^{-11} yr^{-1} (see Figure 2; this represents a reduction in length of day of about 1.7 μs/yr).

This paper has also been concerned with a detailed analysis of the sensitivity of the $\dot{J}_\ell$ data to variations in the radial viscosity profile in Earth's mantle, as inferred from forward analyses and calculations of Fréchet kernels. For any given Earth model we have found that the depth range over which a particular $\dot{J}_\ell$ datum is most sensitive to variations in viscosity will generally trend towards shallower regions as the spherical harmonic degree is increased. As an example, for the case of our standard Earth model (ν_{UM} = 10^{21} Pa s, ν_{LM} = 3 x 10^{21} Pa s) the $\dot{J}_\ell$ data, $\ell \leq 4$, are sensitive to variations in viscosity over the entire mantle extending to its deepest regions, while the $\dot{J}_\ell$, $\ell > 4$, are less sensitive to very deep mantle rheology and more sensitive to variations in the upper mantle viscosity.

For Earth models with ν_{UM} = 10^{21} Pa s, predictions of the $\dot{J}_\ell$ harmonics exhibit a pronounced peak when a wide enough region

of ν_{LM} space is considered. We have denoted the lower mantle viscosity of the Earth model associated with this peak value as $\hat{\nu}^{\ell}_{LM}$. Fréchet kernels computed for the case ℓ=2 and ℓ=4 indicate that the sensitivity of the data to variations in mantle rheology is fundamentally altered as ν_{UM} is increased from 10^{21} Pa s to 10^{23} Pa s. For the case of ℓ=2 the kernels reflect a migration of the dominant sensitivity of the data to viscosity variations in regions below about 1200 km depth (for Earth models with $\nu_{LM} < \hat{\nu}^{2}_{LM} = 2 \times 10^{22}$ Pa s) to regions above this depth in the lower mantle (for Earth models with $\nu_{LM} \geq \hat{\nu}^{2}_{LM}$). The stationary point evident in the forward predictions for $\dot{J}_2$ occurs when the two sensitivities are matched. As ν_{LM} is increased further (to approximately 10^{24} Pa s) the $\dot{J}_2$ predictions become insensitive to small viscosity variations anywhere in the lower mantle. The kernels for the $\dot{J}_4$ datum reflect similar trends, with the exception that the stationary point at $\hat{\nu}^{4}_{LM}$ does not arise as a consequence of competing sensitivities, but rather from a null in the sensitivity of the datum to variations in viscosity anywhere in the lower mantle (see Figure 6, top frame).

The sensitivity of the $\dot{J}_{\ell}$ data to variations in the viscosity profile in the shallowest parts of the lower mantle, for the case $\nu_{LM} \geq \hat{\nu}^{\ell}_{LM}$, is reflected in the forward predictions given on Figure 3. The dashed lines on that figure represent predictions for Earth models in which the viscosity above 1200 km depth is constrained to be 10^{21} Pa s, and it is clear in this case that ambiguities in the deep mantle viscosity solutions do not develop. The same is true for forward predictions in which the upper mantle viscosity is weakened an order of magnitude to $\nu_{UM} = 10^{20}$ Pa s and ν_{LM} is varied (dotted lines, Figure 3). Not surprisingly, in this set of Earth models the dominant sensitivity of the $\dot{J}_{\ell}$ data, to variations in the viscosity profile, is concentrated in the upper mantle (the evolution of sensitivity arising from a weakening of ν_{UM} is apparent in the bottom frames of Figures 5 and 6).

These arguments represent specific cases of one of the more general conclusions of this study. The sensitivity of the $\dot{J}_{\ell}$ zonal harmonics to variations in the radial mantle viscosity profile, is a strong function of the viscosity model. Some generalizations are certainly valid, for example that the zonal harmonics $\dot{J}_{\ell}$, $\ell > 4$, are very sensitive to upper mantle rheology, however even in this case the detailed radial variation in the sensitivity of the data will be a strong function of the viscosity variation above 670 km depth. Conclusions regarding the sensitivity of the $\dot{J}_{\ell}$ data to variations in mantle viscosity must be associated with a particular class of Earth models.

The potential sensitivity of the $\dot{J}_{\ell}$ data to variations in the viscosity of the shallowest regions of the mantle (in particular, see Figure 4, for $\ell > 4$) raises another important issue. The calculations performed in this study assume an Earth model with a lithospheric thickness of 120 km. Variations in that parameter may have a non-negligible effect on the predictions, especially for $\ell \geq 4$ (but see *Peltier* [1984] for a discussion of the $\ell = 2$ case).

A final consideration of the sensitivity of the zonal harmonics $\dot{J}_{\ell}$ to variations in the radial mantle viscosity profile must be generated within the framework of an inverse theory applied to the observed data. That is, the resolving power of the data (or datum) can be assessed once a model is established which is consistent with the observations. The theory for the computation of Fréchet kernels, derived and applied in this study, will permit this application.

We have applied our theory to compute the $\dot{J}_{\ell}$ signal (for $\ell \leq 10$) arising from the retreat of 31 smaller ice sheets and glaciers analyzed by *Meier* [1984], and also from any potential mass variations in the Antarctic and Greenland ice sheets. We have found that the $\dot{J}_{\ell}$ signal from ongoing glacial isostatic adjustment in consequence of the late Pleistocene glacial cycles will dominate the signal from Meier's sources at all degrees except 3 (between degrees 4 and 8 the signal from the former is at least an order of magnitude higher than that from the latter). The $\dot{J}_2$ signal contributed by Meier's sources is the same magnitude, and opposite in sign, as the maximum signal contributed by the ocean syphoning phenomenon.

The $\dot{J}_{\ell}$ signal arising from mass variations in the Antarctic and Greenland ice sheets is potentially comparable to the glacial isostatic adjustment signal. This indicates that a comparison of observational constraints on the $\dot{J}_{\ell}$ data with predictions of the sort described in section 3, with the goal of constraining mantle rheology, will be useless unless constraints are placed on the signal from present-day variations in the mass of the Antarctic and Greenland ice sheets. The required constraints are weakest at ℓ=2, and to a lesser extent ℓ=4, where only the net mass flux from the two ice sheets needs to be known accurately. At other degrees the efficiency of mass variations in the Antarctic and Greenland ice sheets in exciting a $\dot{J}_{\ell}$ response diverges and the mass flux from each ice sheet must be ascertained independently. At degrees above ℓ=3 the situation is complicated further by the fact that the $\dot{J}_{\ell}$ signal is sensitive, at these degrees, to the space dependence of the mass variations on the two ice sheets.

Finally, we have outlined a procedure in which predictions of the present-day $\dot{J}_{\ell}$ signal due to the late Pleistocene glacial cycles, as well as from Meier's sources, may be used in conjunction with an observational constraint on $\dot{J}_2$, to derive bounds on the net present day mass flux from the Antarctic and Greenland ice sheets to the global oceans. If *Rubincam's* [1984] estimate of $\dot{J}_2$ ($2.58 \pm 0.57 \times 10^{-11}$ yr^{-1}) is correct (the estimate is now under critical review), then the results of Figures 3 and 7 indicate that the net mass balance on the Antarctic and Greenland ice sheet is contributing a eustatic sea level rise in the range -0.25 to 1.25 mm/yr. This range can be substantially reduced by invoking independent constraints on the mantle viscosity profile. We must emphasize, however, that the re-establishment of rigorous observational constraints on the $\dot{J}_{\ell}$ harmonics, which should be possible in the next few years, is fundamental to an application of the results described in this paper to studies involving inferences of mantle rheology and constraints on present day global sea level change.

Acknowledgments. The work reported in this paper was supported in part by a grant to W.R.P. from the Climate and Global Change Program of the U.S. National Oceanic and Atmospheric Administration (NOAA) in the area of Global Sea Level. It is part of a project to develop an ultra-high-resolution model of the postglacial rebound process for use in the "decontamination" of tide gauge data. The rotational constraints on such models are clearly rather important. The research of J.X.M. at Harvard-Smithsonian has been supported in part by NSERC, the Smithsonian Institution and NASA grant NAG5-1930. The research of W.R.P. at the University of Toronto is also supported by NSERC grant A9627. We thank J.L. Davis and A.M. Forte for their many constructive comments related to this research.

REFERENCES

Carter, W.E., and D.S. Robertson, Greenland ice sheet: Is it growing or shrinking?, *Science, 248*, 288-289, 1990.

Cathles, L.M., The viscosity of the earth's mantle, Ph.D. Thesis, Princeton Univ., Princeton, N.J., 1971.

Cathles, L.M., *The Viscosity of the Earth's Mantle*, Princeton University Press, Princeton, N.J., 1975.

Chappell, J., and N.J. Shackleton, Oxygen isotopes and sea level, *Nature*, *324*, 137-140, 1986.

Cheng, M.K., R.J. Eanes, C.K. Shum, B.E. Schutz, and B.D. Tapley, Temporal variations in low degree zonal harmonics from Starlette orbit analysis, *Geophys. Res. Lett.*, *16*, 393-396, 1989.

Clark, J.A., W.E. Farrell, and W.R. Peltier, Global changes in postglacial sea level: A numerical calculation, *Quat. Res.*, *9*, 265-287, 1978.

Currot, D.R., Earth deceleration from ancient solar eclipses, *Astron. J.*, *71*, 264-269, 1966.

Davis, J.L., J.X. Mitrovica and I.I. Shapiro, Determination of tidal parameters from an extensive VLBI data set, *EOS Trans. AGU*, *72*(44), 113, 1991.

Douglas, B.C., Global sea level rise, *J. Geophys. Res.*, *96*, 6981-6992, 1991.

Dziewonski, A.M. and D.L. Anderson, Preliminary Reference Earth Model (PREM), *Phys. Earth Planet. Inter.*, *25*, 297-356.

Etkins, R., and E.S. Epstein, The rise of global mean sea level as an indication of climate change, *Science*, *215*, 287-288, 1982.

Forte, A.M., and W.R. Peltier, Plate tectonics and aspherical Earth structure: The importance of poloidal-toroidal coupling, *J. Geophys. Res.*, *92*, 3645-3679, 1987.

Garland, G.D., *Introduction to Geophysics - Mantle, Core and Crust*, W.B. Saunders, Philadelphia, Pa., 1979.

Haskell, N.A., The motion of a viscous fluid under a surface load, 2, *Physics*, *7*, 56-61, 1936.

Herring, T.A., Very long baseline interferometry, in *Space Geodesy and Geodynamics*, A.J. Anderson, pp. 169-196, *Academic*, San Diego, Calif., 1986.

Marsh, J.G., et al., The GEM-T2 gravitational model, *J. Geophys. Res.*, *95*, 22,043-22,071, 1990.

McConnell, R.K., Viscosity of the mantle from relaxation time spectra of isostatic adjustment, *J. Geophys. Res.*, *73*, 7089-71-5, 1968.

Meier, M.F., Contribution of small glaciers to global sea level, *Science*, *226*, 1418-1421, 1984.

Mitrovica, J.X., and W.R. Peltier, Pleistocene deglaciation and the global gravity field, *J. Geophys. Res.*, *94*, 13,651-13,671, 1989.

Mitrovica, J.X., and W.R. Peltier, Free air gravity anomalies associated with glacial isostatic disequilibrium: Load history effects on the inference of deep mantle viscosity, *Geophys. Res. Lett.*, *18*, 235-238, 1991*a*.

Mitrovica, J.X. and W.R. Peltier, On postglacial geoid subsidence over the equatorial oceans, *J. Geophys. Res.*, *96*, 20,053-20,071, 1991*b*.

Mitrovica, J.X., and W.R. Peltier, A complete formalism for the inversion of post-glacial rebound data: resolving power analysis, *Geophys. J. Int.*, *104*, 267-288, 1991*c*.

Mitrovica, J.X., and W.R. Peltier, The inference of mantle viscosity from an inversion of the Fennoscandian relaxation spectrum, *Geophys. J. Int.*, in press, 1992.

Peltier, W.R., The impulse response of a Maxwell Earth, *Rev. Geophys.*, *12*, 649-669, 1974.

Peltier, W.R., Glacial isostatic adjustment, II, The inverse problem, *Geophys. J. R. Astron. Soc.*, *46*, 669-706, 1976.

Peltier, W.R., Dynamics of the ice age earth, *Advances in Geophysics*, *24*, 1-146, 1982.

Peltier, W.R., Constraint on deep mantle viscosity from LAGEOS acceleration data, *Nature*, *304*, 434-436, 1983.

Peltier, W.R., The LAGEOS constraint on deep mantle viscosity: Results from a new normal mode method for the inversion of viscoelastic relaxation spectra, *J. Geophys. Res.*, *90*, 9411-9421, 1985.

Peltier, W.R., Global sea level and Earth rotation, *Science*, *240*, 895-901, 1988.

Peltier, W.R., and J.T. Andrews, Glacial isostatic adjustment, I, The forward problem, *Geophys. J. R. Astron. Soc.*, *46*, 605-646, 1976.

Peltier, W.R., R.A. Drummond, and A.M. Tushingham, Post-glacial rebound and transient lower mantle rheology, *Geophys. J. R. Astron. Soc.*, *87*, 79-116, 1986.

Peltier, W.R., A.M. Forte, J.X. Mitrovica, and A.M. Diziewonski, Mantle convection and the free-air gravity anomaly over Laurentia, *EOS Trans. AGU*, *72*, 507, 1991.

Peltier, W.R., A.M. Forte, J.X. Mitrovica, and A.M.Dziewonski, Earth's gravitational field: Seismic tomography resolves the enigma of the Laurentian anomaly, *Geophys. Res. Lett.*, *19*, 1555-1558, 1992.

Peltier, W.R., and A.M. Tushingham, Global sea level rise and the greenhouse effect: Might they be connected?, *Science*, *244*, 806-810, 1989.

Ricard, Y., and C. Vigny, Mantle dynamics with induced plate tectonics, *J. Geophys. Res.*, *94*, 17,543-17,559, 1989.

Richards, M.A., and B.H. Hager, Geoid anomalies in a dynamic Earth, *J. Geophys. Res.*, *89*, 5987-6002, 1984.

Richards, M.A. and B.H. Hager, The Earth's geoid and the large-scale structure of mantle convection, in *The Physics of Planets*, edited by S.K. Runcorn, pp. 247-272, John Wiley, New York, 1988.

Rubincam, D.P., Postglacial rebound observed by LAGEOS and the effective viscosity of the lower mantle, *J. Geophys. Res.*, *89*, 1077-1087, 1984.

Sabadini, R., D.A. Yuen, and P. Gasperini, Mantle rheology and satellite signatures from present-day glacial forcings, *J. Geophys. Res.*, *93*, 437-447, 1988.

Shackleton, N.J., A. Berger, and W.R. Peltier, An alternative astronomical calibration of the lower Pleistocene timescale based upon ODP site 677, *Trans. R. Soc. Edinburgh Earth Sci.*, *81*, 251-261, 1990.

Trupin, A.S., M.F. Meier, and J.M. Wahr, Effect of melting glaciers on the Earth's rotation and gravitational field: 1965-1984, *Geophys. J. Int.*, *108*, 1-15, 1992.

Tushingham, A.M., and W.R. Peltier, ICE-3G: A new global model of late Pleistocene deglaciation based upon geophysical predictions of postglacial relative sea level change, *J. Geophys. Res.*, *96*, 4497-4523, 1991.

Tushingham, A.M. and W.R. Peltier, Validation of the ICE-3G model of Würm-Wisconsin deglaciation using a global data base of relative sea level histories, *J. Geophys. Res.*, *97*, 3285-3304, 1992.

Wu, P. and W.R. Peltier, Glacial isostatic adjustment and the free air gravity anomaly as a constraint on deep mantle viscosity, *Geophys. J.R. Astron. Soc.*, *74*, 377-450, 1983.

Wu, P., and W.R. Peltier, Pleistocene deglaciation and the Earth's rotation: A new analysis, *Geophys. J.R. Astron. Soc.*, *76*, 753-791, 1984.

Yoder, C.F. and E.R. Ivins, Changes in the Earth's gravity field from Pleistocene deglaciation and present-day glacial melting, *EOS Trans. AGU*, *66*(18), 245, 1985.

Yoder, C.F., J.G. Williams, J.O. Dickey, B.E. Schutz,R.J. Eanes, and B.D. Tapley, $\dot{J}_2$ from LAGEOS and the non-tidal acceleration of Earth rotation, *Nature*, *303*, 757-762, 1983.

Yuen, D.A., P. Gasperini, R. Sabadini, and E. Boschi, Azimuthal dependence in the gravity field induced by recent and past cryospheric forcings, *Geophys. Res. Lett.*, *14*, 812-815, 1987.

Yuen, D.A. and R. Sabadini, Viscosity stratification of the lower mantle as inferred from the $\dot{J}_2$ observation, *Ann. Geophys.*, *3*, 647-654, 1985.

Zumberge, M.A., R.L. Rinkler, and J.E. Faller, A portable apparatus for absolute measurements of the Earth's gravity, *Metrologia*, *18*, 145-152, 1982.

Zwally, H.J., Growth of Greenland ice sheet: Interpretation, *Science*, *246*, 1589-1591, 1989.

J. X. Mitrovica and W. R. Peltier, Department of Physics, University of Toronto, Toronto, Ontario, Canada M5S 1A7.

(Received April 8, 1992;
revised November 2, 1992;
accepted November 11, 1992.)